Aquatic metabolism influences temporal variations of water carbon and atmospheric carbon dioxide fluxes in a temperate salt marsh

Jérémy Mayen[1,2,3], Pierre Polsenaere[1], Aurore Regaudie de Gioux[4], Jonathan Deborde[1], Karine Collin[2], Yoann Le Merrer[2], Élodie Foucault[5], Vincent Ouisse[5], Laurent André[6,7], Marie Arnaud[1], Pierre Kostyrka[1], Éric Lamaud[8], Gwenaël Abril[9], Philippe Souchu[2]

[1]Ifremer, COAST, F-17390 La Tremblade, France
[2]Ifremer, COAST, F-44000 Nantes, France
[3]Univ. Bordeaux, CNRS, Bordeaux INP, EPOC, UMR 5805, F-33600 Pessac, France
[4]Ifremer, DYNECO, F-29280 Plouzané, France
[5]MARBEC, Univ. Montpellier, CNRS, Ifremer, IRD, F-34200 Sète, France
[6]BRGM, F-45060 Orléans, France
[7]ISTO, UMR7327, Univ. Orléans, CNRS, BRGM, OSUC, F-45071 Orléans, France
[8]INRAE, Bordeaux Sciences Agro, ISPA, F-33140 Villenave d'Ornon, France
[9]Laboratoire de Biologie des Organismes et Ecosystèmes Aquatiques (BOREA), UMR 8067, Muséum National d'Histoire Naturelle, CNRS, IRD, SU, UCN, UA, Paris, France

Correspondence to: Jérémy Mayen (jeremy.mayen@bordeaux-inp.fr).

Abstract. Salt marshes are blue carbon (C) ecosystems characterized by intense atmospheric CO_2 uptake and C sequestration but also organic and inorganic C exports through the tide. However, uncertainties on main factors controlling vertical and horizontal C fluxes imply studying simultaneously terrestrial and aquatic metabolisms at small timescales (diurnal and tidal) and distinguish their contributions to net ecosystem CO_2 exchanges (NEE). Within a temperate salt marsh, four sampling 24-h cycles were performed to measure water biogeochemical parameters (carbon and nutrients) and planktonic metabolism simultaneously to NEE from high tide during marsh immersion (imported coastal waters influenced by the continental shelf) to low tide during marsh emersion (exported channel waters influenced by the marsh drainage). At high tide, water CO_2 oversaturation due to marsh aquatic heterotrophy and CO_2-concentrated water inputs from the coastal end-member induced water-air CO_2 emissions during marsh immersion. At low tide, water pCO_2 were also mainly controlled by marsh biological activity inducing large water CO_2 oversaturation in winter due to heterotrophy and large water CO_2 undersaturation in spring and summer due to autotrophy. In winter, the highest increases of dissolved inorganic carbon (DIC; from 2354 to 3963 µmol kg^{-1}), total alkanity (TA; from 2508 to 4016 µmol kg^{-1}) and dissolved inorganic nitrogen (DIN; from 27.7 to 68.4 µM) were measured simultaneously at low tide night probably due to intense anaerobic respiration processes in channel waters and/or sediments resulting in the highest water pCO_2 increase (from 533 to 1461 ppmv). On the contrary, in spring and summer, large water pCO_2 decreases (down to 83 ppmv) and dissolved organic carbon (DOC) increases (up to 1040 µM) from high to low tide could be related to intense autochthonous and allochthonous marsh primary production, including benthic microalgae, phytoplankton and macroalgae. This study suggests that the horizontal exchanges of coastal waters with the salt marsh significantly participate to measured water carbon dynamics and associated channel water CO_2 sink/source status,

through strong biological activity in the salt marsh (production and respiration). At the daily scale, plant and phytoplankton metabolisms played a major and a minor role, respectively, to the marsh CO_2 sink measured at the ecosystem scale (NEE), even during low immersion where emerged plants located on the highest marsh levels can maintain CO_2 uptake despite aquatic heterotrophy and shelf-contributed CO_2 emissions.

1. Introduction

Atmospheric CO_2 emissions by anthropogenic activities have strongly modified the biogeochemical equilibrium of the global carbon (C) cycle favouring global warming and sea level rise (Friedlingstein et al., 2023). Significant amounts of anthropogenic CO_2 have been uptaked by marine environments via CO_2 solubilisation in seawater and phytoplankton photosynthesis. However, uncertainties yet remain on the redistribution of these CO_2 fluxes and associated processes, particularly within the vegetated coastal systems such as salt marshes (Bauer et al., 2013; Cai, 2011). Indeed, salt marshes are among the most productive ecosystems in the biosphere with net ecosystem production (NEP) rates of 382 g C m^{-2} yr^{-1} (Alongi, 2020) and 448 g C m^{-2} yr^{-1} (Wang et al., 2024), which means they act as significant CO_2 sinks (Cai, 2011). A part of marsh primary production (~8%) can be buried in sediments as "blue carbon" (Chmura et al., 2003; Song et al., 2023) helping to offset anthropogenic CO_2 emissions. Blue carbon burial rates in vegetated coastal systems such as salt marshes (218 ± 24 g C m^{-2} yr^{-1}), mangroves (226 ± 39 g C m^{-2} yr^{-1}) and seagrass beds (138 ± 38 g C m^{-2} yr^{-1}), are among the highest on Earth, and thus significantly contribute (per surface units) to the global carbon cycle in comparison with terrestrial ecosystems (Adame et al., 2024; Mcleod et al., 2011). The majority of marsh primary production (> 70%) is respired and exported out of the system through horizontal and vertical carbon fluxes whose dynamics strongly depend on seasonal, diurnal and tidal rhythms (Nakamura et al., 2024; Song et al., 2023; Wang et al., 2016). Various respiration processes in marsh sediments and waters produce and export large quantities of dissolved inorganic carbon (DIC) and total alkalinity (TA) by tides, thus influencing in turn partial pressures of CO_2 (pCO_2) or more generally, the carbonate system of tidal waters (Reithmaier et al., 2023; Santos et al., 2021; Wang et al., 2016) and the carbon balance of downstream coastal systems (Bauer et al., 2013; Cai, 2011). The second pathway for marsh carbon loss are atmospheric CO_2 emissions from emerged and immersed marsh respiration (Song et al., 2023). Consequently, the strong heterogeneity of horizontal and vertical carbon fluxes in salt marshes caused by seasonal, diurnal and tidal rhythms (Song et al., 2023; Wang et al., 2018) requires simultaneous integrative measurements of net ecosystem CO_2 exchanges (NEE) and organic and inorganic carbon in tidal waters to better evaluate all marsh carbon processes and fluxes at the various temporal and spatial scales.

In terrestrial ecosystems, NEE measured by atmospheric Eddy Covariance (EC) generally correspond to NEP (Chapin et al., 2006; Kowalski et al., 2003). However, in salt marshes, the latter relationship is more complex and NEE does not fully correspond to NEP since lateral DIC exports are not recorded by EC measurements, especially during flood and ebb tides (Mayen et al., 2024; Wang et al., 2018). During marsh emersion, NEE mainly occurs at the soil-atmosphere interface, implying a strong contribution from benthic NEP (plants and sediments) to atmospheric CO_2 exchanges (Forbrich and Giblin, 2015; Schäfer et al., 2014). For example, in a French vegetated salt marsh, high rates of primary production and

respiration induced a yearly CO_2 uptake during daytime emersion (-3.86 ± 3.62 µmol m^{-2} s^{-1}) and a yearly CO_2 emission during night-time emersion (1.22 ± 1.18 µmol m^{-2} s^{-1}; Mayen et al., 2024). In addition, microphytobenthos (MPB) in sediments, composed of benthic microalgae, can migrate to the surface of muddy sediments during daytime emersion to use photosynthetically active radiation and contribute as well to benthic NEP (Migné et al., 2007; Xi et al., 2019). Conversely, marsh sediments can also behave as a net source of atmospheric CO_2, especially during the non-growing season for plants, mainly due to predominant microbial decomposition of soil organic matter (Gong et al., 2023). During marsh immersion, advected coastal waters create a physical barrier between benthic and atmospheric compartments which strongly influences NEE (Chapin et al., 2006; Mayen et al., 2024). In this situation, NEE combines cumulated contributions from benthic NEP, planktonic NEP and horizontal carbon exchanges through the tide. In addition, during immersion, organic carbon produced at emersion can be transferred to the water column and contribute to planktonic NEP, such as MBP (Polsenaere et al., 2012; Savelli et al., 2019). The shallowness of coastal environments can favour simultaneously both high primary production rates of planktonic communities due to significant light penetration in water (Gazeau et al., 2004) and also strong water-sediment DIC exchanges (Gong et al., 2023; Wang et al., 2016; Wang and Cai, 2004). Previous studies in salt marshes highlight atmospheric CO_2 emissions during immersion due to heterotrophic metabolism in tidal waters (Song et al., 2023; Wang et al., 2018). However, few studies show the contribution of water CO_2 and planktonic communities on marsh metabolic fluxes at the ecosystem scale. Therefore, it is important to study more precisely the whole marsh metabolism integrating terrestrial and aquatic compartments at the different spatio-temporal scales and pinpointing their respective contributions to net ecosystem CO_2 exchanges (sink/source) to better take into account salt marshes in regional and global carbon balances.

At a temperate salt marsh, this present study focuses on aquatic metabolism influence on water carbon dynamics and net ecosystem CO_2 exchanges at small timescales (diurnal and tidal) during the four seasons. The main aims of this paper are (1) to highlight biotic and abiotic controlling factors on water carbon variations, in particular water pCO_2, (2) to study the metabolic status of planktonic communities in the marsh as CO_2 sink or source and (3) to identify the contribution of water pCO_2 signature and planktonic/water column metabolism on NEE. To this purpose, we performed four seasonal 24-hour cycles (continuous samplings for 24 hours) measuring relevant water biogeochemical parameters (pCO_2, organic and inorganic carbon and nutrients), planktonic metabolism and water-air CO_2 fluxes at a single point in the main channel of the salt marsh connected to upstream salt ponds and downstream continental shelf. The novelty of this study was to look for marsh aquatic metabolism contribution on water carbon dynamics and water-air CO_2 fluxes, using *in situ* carbon original samplings through 24-h cycles at each season simultaneously with large scale and continuous atmospheric CO_2 exchange measurements (NEE by Eddy Covariance).
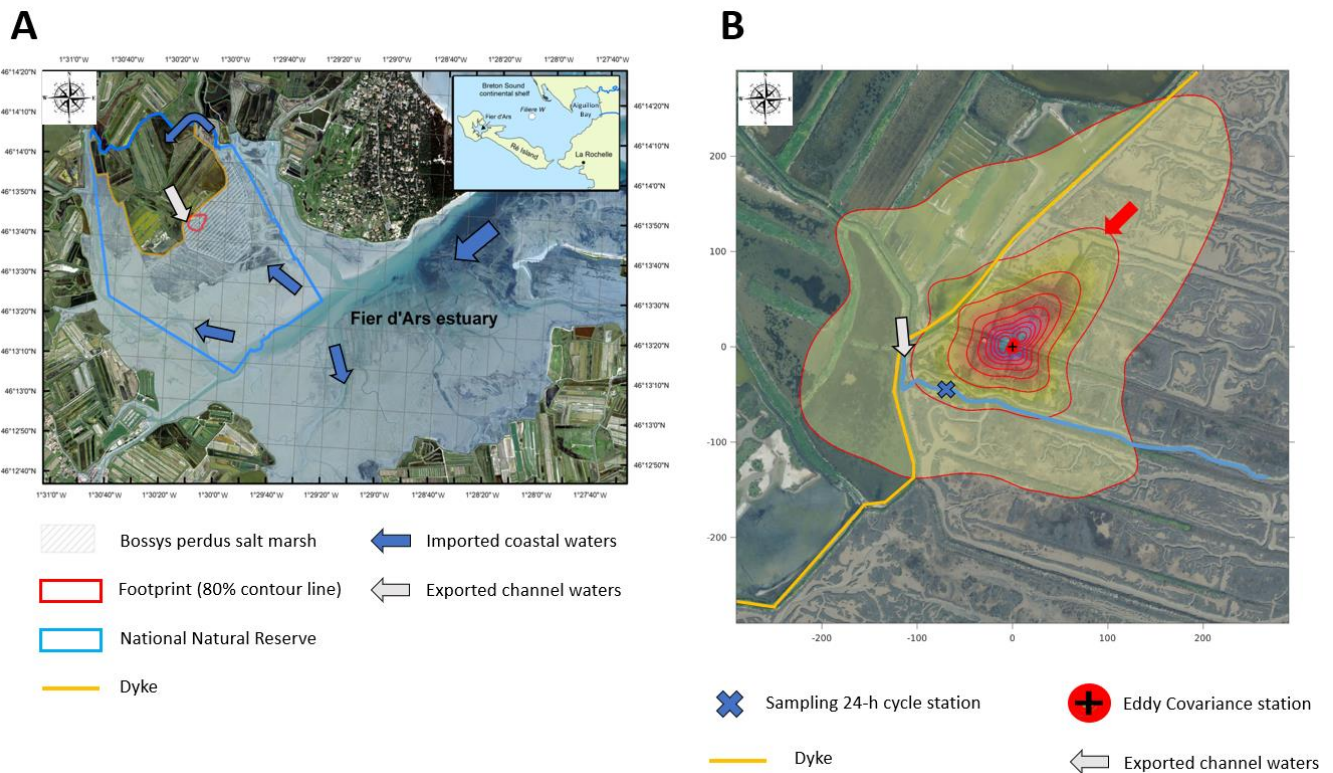
Fig. 1. (A) The Bossys perdus salt marsh located on the French Atlantic coast on Ré Island within the National Natural Reserve. This tidal salt marsh is connected to the downstream Fier d'Ars estuary (light blue tidally immerged area) and upsteam artificial salt marshes (i.e. salt ponds). The dyke (orange line) separates terrestrial and maritime marsh areas. Blue arrows represent coastal water inputs from the estuary and the continental shelf at high tide (tidal marsh flooding and salt pond supplying) and grey arrows represents exported waters at low tide from salt ponds to the estuary through the main studied channel. The studied footprint area (80% countour line) of the Bossys perdus marsh is indicated (red line). **(B)** Location and set-up of the Eddy Covariance system within the Bossys perdus salt marsh at low tide (marsh emersion) and its associated footprints averaged over the year 2021. The red arrow indicates the studied footprint countour line encompassing the water sampling location (blue cross). From geo-referenced IGN orthogonal images (IGN, 2019).

2. Materials and methods

2.1. Study site

The Bossys perdus salt marsh is a vegetated intertidal wetland (52.5 ha) located along the French Atlantic coast on Ré Island (Fig. 1-A). The salt marsh is located within the Fier d'Ars tidal estuary which receives coastal waters from the Breton Sound continental shelf during high tide periods (Fig. 1-A). This intercommunication enables (1) the immersion of the estuarine intertidal zone (including the studied salt marsh) and (2) the water supply for artificial salt marshes (i.e. salt ponds) upstream of the dyke. Water residence times in the salt ponds vary from a few hours to a fortnight depending on seasonal management practice. Generally, macroalgae blooms (*Ulva* spp.) colonize salt ponds from April to October each year (Mayen et al., 2023). After an intensive land-use (salt harvesting and oyster farming), the Bossys perdus salt marsh is now protected within a National Natural Reserve to restore its natural hydrodynamics and vegetation while conserving the site's

4

120   specific typology due to past human activities (channel networks, humps and dykes; Fig. 1-B) (Mayen et al., 2024). Two different substrata can be found in the soil of the salt marsh with sand-dominated sediments at bottom and mud-dominated sediments at top (transition depth at 33 cm). In the muddy section, dry bulk density and organic carbon content were 0.8 ± 0.1 g cm^{-3} and $1.78 \pm 0.19\%$, respectively (Amann et al., 2024). The salt marsh is subject to semi-diurnal tides originating on the continental shelf allowing its immersion through channels differently in space, time and frequency depending on tidal

125   periods. At high tide (HT), imported coastal waters gradually fill the sampling channel (Fig. 1-B) and immerse the salt marsh at variable water heights depending on tidal amplitudes and meteorological conditions. Due to the site's specific typology, lowest marsh levels (mudflats and *S. maritima*) were quickly immersed (south), whereas the whole marsh immersion (all muds and plants) only occurred 0.75 h later at the highest water heights (Mayen et al., 2024). At low tide (LT), the channel empties and the salt marsh is emerged and exposed to the atmosphere. During this time, water remaining at the bottom of the

130   channel come from (i) the Bossys perdus marsh-drainage process by tidal pumping and (ii) the waterflow from the upstream salt ponds to the downstream estuary (Fig. 1-B) at low water height situations (0.50 m maximum depth; see Fig. S1 in Mayen et al., 2024) fluctuating seasonally according to meteorological conditions and pond managements (Mayen et al., 2023).

135   ## 2.2. Sampling strategy and field samplings

At a single point in the main channel of the salt marsh (Fig. 1-B), four seasonal 24-h cycles were performed from March to December 2021 (Fig. 2). For each 24-h cycle, our sampling strategy consisted of simultaneously measuring water biogeochemical parameters, planktonic metabolism and water-air CO_2 fluxes at diurnal (daytime and night-time) and tidal (from high to low tide and all tidal phases in between) scales through discrete samplings and continuous real-time

140   measurements. At this station, samplings of sub-surface water were performed continuously every one or two hours over the four 24-h cycles (n = 13 over C1-winter, n = 15 over C2-spring and C3-summer and n = 16 over C4-fall) encompassing a large variation in water heights (Hw): from the channel bottom at low tide (Hw = 0.5 m) to the full marsh immersion at high tide (Hw > 2.5 m) with all tidal intermediate situations in between (Fig. 2 and Fig. S1). When repeated across seasons, it allows to sample the full tidal range, and hence the heterogeneity of the tidal height, residence time and water mixing. These

145   discrete samplings allowed the analysis of photosynthetic pigments (Chl*a*), carbonate system parameters (TA), nutrients (NO_3^-, NO_2^-, NH_4^+, DIP and DSi) and organic matter parameters (DOC, POC and PON) (Table 1). Water samples were collected using a 5 L glass bottle, directly filtered in the field and conditioned for chemical analysis in the laboratory. For organic matter, sampling equipment was pre-washed with HCl 10% (for 12h), rinsed with deionised water and dried (Lorrain et al., 2003). The glassware and GF/F filters were pre-combusted (for 4h at 450°C). For planktonic metabolism

150   measurements, water samples were collected every six hours during each 24-h cycle (n = 4) successively at low tide (LT; water remaining at the channel bottom) and high tide (HT; water flooding mostly marsh surface). At HT, when the marsh is fully flooded, horizontal homogenization of water masses occurs, due to surface water flows induced by complex tidal circulation and wind action. In addition, partial pressure of CO_2 (pCO$_2$), temperature, salinity and dissolved oxygen (DO)

5

were measured every 10-min in sub-surface waters using *in situ* probes. These measurements were also performed at the same frequency in the 4 days before each 24-h cycle. Thus, the successive hourly sampling over 24-hours at LT during marsh emersion (exported channel waters influenced by the marsh) and at HT during marsh immersion (imported coastal waters influenced by the continental shelf) both at day and night allowed to take into account all carbon temporal variability (LT/Day, HT/Day, LT/Night, HT/Night; Fig. 2).

2.3. Continuous parameters

2.3.1. Water pCO_2 measurements and associated physicochemical parameters

At each season, a C-sense[TM] pCO_2 probe (Turner Designs, USA) and an EXO2 multiparameter probe (YSI Inc., USA) were deployed in the sampling channel to continuously measure (every 10-min) *in situ* biogeochemical parameters over 5 days. The measurement range of the C-sense[TM] probe was 0-2000 ppmv with an absolute accuracy of 60 ppmv (3% of the full scale). A water pCO_2 correction was applied taking into account total dissolved gas pressure and atmospheric pressure during calibration (Mayen et al., 2023). The EXO2 probe was used to measure water temperature ($\pm$ 0.1°C), salinity ($\pm$ 0.2 salinity unit), DO concentration ($\pm$ 3.1 µmol L^{-1}) and DO saturation level ($\pm$ 1%). At the same time, water heights ($\pm$ 0.3 m) were measured every 10-min by a STPS probe (NKE Instrumentation, France). Water heights (Hw) measured at one location in the channel relative to the mean sea level were used to distinguish LT periods with constant water heights (Hw = 0.50 m) and HT periods with increases (flood tide) and decreases (ebb tide) in water heights (0.5 < Hw < 2.50 m; Fig. 2).

2.3.2. Atmospheric Eddy Covariance and footprint

Over the year 2021, and simultaneously to our water samplings, an atmospheric Eddy Covariance (EC) system (model EC150, *Campbell Scientific Inc.,* Logan, UT) was deployed at the salt marsh (Fig. 1-B). The EC system continuously measured net ecosystem CO_2 exchanges (NEE, µmol CO_2 m^{-2} s^{-1}) within the annual averaged footprint (80% contour line, 12069 m^2). EC data were recorded at a frequency of 20-Hz and averaged every 10-min over each 24-h cycle except for during C4-fall where no EC measurement was possible due to anemometer maintenance. Photosynthetically active radiation (PAR, µmol m^{-2} s^{-1}), air temperature (Ta, °C), relative humidity (RH, %) and cumulative precipitation (rainfall, mm) were also recorded simultaneously with NEE. Daytime and night-time were separated into PAR > 10 and PAR $\leq$ 10 µmol m^{-2} s^{-1}, respectively (Fig. 2). The set of EC sensors, footprint estimation, EC data processing, quality control and gap-filling model are fully described by Mayen et al. (2024). A habitat covering map showed that the studied footprint was occupied mainly by halophytic plants including *Halimione portulacoides* (37%), *Spartina maritima* (22%) and *Suaeda vera* (7%) whereas, mudflats and channels occupied 34% of the footprint area (Mayen et al., 2024). *H. portulacoides* and *S. vera* are evergreen plants throughout the year whereas, the growing season for *S. maritima* was shorter (from spring to late summer). During winter and fall, *S. maritima* persists only in the form of rhizomes and its low metabolism could induce lower marsh CO_2 uptake rate (Mayen et al., 2024). At the ecosystem scale, NEE < 0 represent a marsh CO_2 uptake (atmospheric sink) and NEE > 0 represent a marsh CO_2 emission (atmospheric source). To study marsh metabolism related to photosynthesis and

respiration processes, NEE were partitioned during LT periods into marsh gross primary production (GPP_{marsh}) and marsh respiration (R_{marsh}), respectively (Kowalski et al., 2003; Wei et al., 2020). In this study, NEE correspond to net ecosystem

190   CO_2 exchanges measured continuously by EC, whereas NEE_{marsh} (GPP_{marsh} - R_{marsh}) correspond to net marsh metabolic fluxes estimated continuously solely at the emerged soil-air interface without immersion (Mayen et al., 2024).
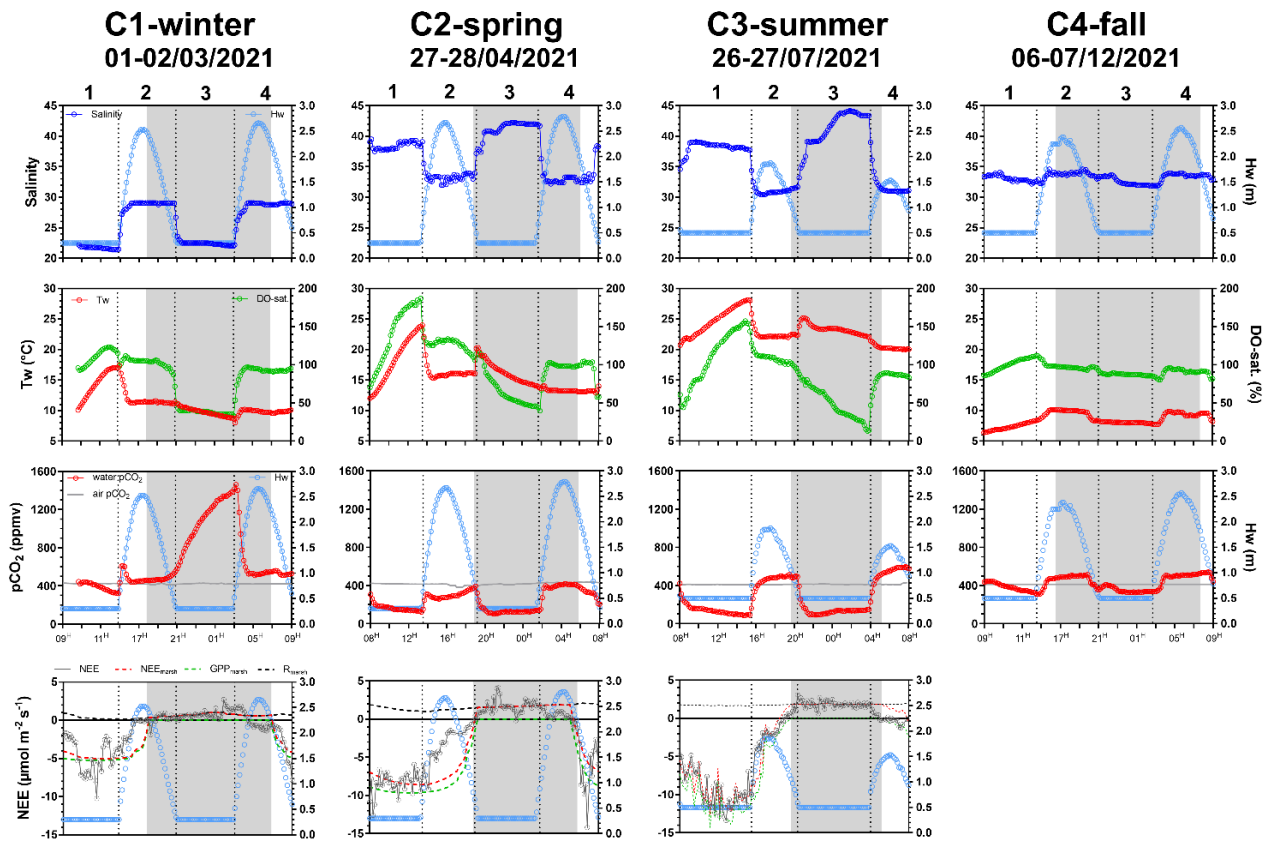

Fig. 2. Temporal variations of biogeochemical parameters measured during the four seasonal 24-h cycles: salinity, water height
195   **(Hw, m), water temperature (Tw; °C), DO saturation level (DO-sat.; %), water pCO_2 (ppmv), air pCO_2 (ppm) and NEE fluxes**
(μmol CO_2 m^{-2} s^{-1}). Estimated NEE_{marsh}, GPP_{marsh} and R_{marsh} fluxes (μmol CO_2 m^{-2} s^{-1}) are presented simultaneously with measured
NEE fluxes. All parameters were measured or estimated every 10-min. during each 24-h cycle. Daytime periods (white areas) and
night-time periods (grey areas) were separated into atmospheric PAR > 10 and atmospheric PAR ≤ 10 μmol m^{-2} s^{-1}, respectively.
No variation of Hw (Hw = 0.50 m) corresponds to low tide and increase/decrease of Hw (0.50 < Hw < 2.50 m) correspond to high
200   **tide (flooding/ebbing). Vertical dotted lines distinguish low tide day (LT/Day, 1), high tide day (HT/Day, 2), low tide night**
(LT/Night, 3) and high tide night (HT/Night, 4). Each graduation of the x-axis corresponds to two hours in universal time.

205

2.4. Analytical procedures

2.4.1. Discrete parameters

For dissolved inorganic nitrogen (DIN = NO_3^- + NO_2^- + NH_4^+) and phosphorus (DIP = PO_4^{3-}), 300 mL water samples were pre-filtered through cellulose acetate membrane filters (Minisart Sartorius© 0.45 µm pore size) directly after sampling and stored at -20°C pending analysis. For dissolved silicate (DSi = $Si(OH)_4^-$), 100 mL filtered water samples were stored at 4°C pending analysis. Samples were analysed using an auto-analyser (Seal analytical AA3) following standard protocols (Aminot and Kérouel, 2007). Nitrate and nitrite were analysed together and grouped as $NO_3^-\_NO_2^-$. The limits of quantification were 0.4 µM for DSi, 0.2 µM for $NO_3^-\_NO_2^-$ and 0.05 µM for DIP and NH_4^+. Measurement uncertainties were 4% for DSi and 8% for $NO_3^-\_NO_2^-$, NH_4^+ and DIP and were obtained from certified reference material comparisons within interlaboratory studies (the Dutch Accreditation Council, ISO 17043:2010). Total alkalinity (TA) analyses were performed using an automatic titration system (Titroline 7000 from SI Analytics) using HCl 0.01 N on 25 g of filtered samples (Dickson et al., 2007). The equivalent point for TA measurement was calculated by linearizing the Gran function (Gran, 1952). Measurements were compared to certified reference material (CRM, provided by A. G. Dickson from Scripps Institution of Oceanography). The maximal precision level was ± 0.44%.

For dissolved organic carbon (DOC), 50 mL water samples were filtered through pre-combusted GF/F filters (Whatman® Nuclepore™, 0.7 µm pore size) in opaque vials using a glass syringe. Firstly, total carbon concentration was measured using the 680°C combustion catalytic oxidation method on a TOC meter (Shimadzu TOC-LCPH/CPN™). Moreover, by acidifying the sample (HCl, pH < 3.0), inorganic carbon was converted to CO_2 and measured using an infrared gas analyser (Shimadzu TOC-LCPH/CPN™). DOC concentrations were then calculated by the difference between total carbon and inorganic carbon concentrations. For particulate organic carbon (POC) and nitrogen (PON), 30–200 mL water samples were carefully filtered through pre-combusted GF/F filters (Whatman® Nuclepore™). Filters were dried (12 h at 60°C), enclosed within clean glass vials, stored in the dark and protected from humidity pending analysis (Lorrain et al., 2003). After removal of carbonates with phosphoric acid, filters were treated using a CHN element analyser (Thermo Fisher Scientific, Waltham, USA) to measure POC and PON concentrations following Aminot and Kérouel (2004). The analysis of POC stable isotope ratios (δ^{13}C-POC) was performed using an Elemental Analyser Isotope Ratio Mass Spectrometer (EA-IRMS: Thermo Flash HT/EA and Delta V Advantage) following Razanamahandry et al. (2024).

Phytoplankton biomass was estimated through Chl*a* concentrations. Water samples (30–200 mL) were filtered through GF/F filters (Whatman® Nuclepore™) and stored at -20°C pending analysis. Chl*a* was extracted in 10 mL of 90% acetone in the dark at 4°C for 12 hours and analysed by monochromatic spectrophotometry (Aminot and Kérouel, 2004). Microphytoplankton (>20 µm) abundance and community diversity were assessed using an inverted microscope (Zeiss, Axio Observer). 1000 mL water samples were fixed with Lugol iodine solution (2%) and stored in the dark at 4°C. Samples were carefully homogenised before settling in 10 mL sub-sample for 12 hours in Hydro-Bios counting chambers (Utermöhl, 1958). The limit of quantification was 100 cells L^{-1}. To measure bacterial and phytoplanktonic abundances by flow

cytometry, 2 mL water samples were fixed with glutaraldehyde (0.25% final concentration; SIGMA-ALDRICH) and stored

240   at -80°C until analysis. Enumeration was carried out using a flow cytometer (NovoCyte, Agilent Tech.).

2.4.2. Planktonic metabolism

To measure planktonic net ecosystem production (NEP_{pk}), planktonic gross primary production (GPP_{pk}) and planktonic respiration (R_{pk}), 5 L water samples were pre-filtrated through 100 µm pores to remove larger grazers, larges particles or large phytoplankton colonies and carefully siphoned into fifteen 125 mL narrow-mouth Winkler glass bottles

245   with a silicon tube to avoid air oxygen bubbles. Water samples were protected from solar irradiation during the filling of bottles. Five replicate bottles were used to determine the initial oxygen concentrations and five transparent "light" and five opaque "dark" replicate bottles were incubated for six hours in surface water of the sampling channel under *in situ* temperature and PAR to measure changes in oxygen concentration linked to planktonic metabolism (Carpenter, 1965; Carritt

250   and Carpenter, 1966). Dissolved oxygen concentration was measured using the spectrophotometric Winkler approach which shows a standard deviation of 0.45% for inter-repeatability and 0.73% for reproducibility close to 250 µmol L^{-1} (Labasque et al., 2004). NEP_{pk} and R_{pk} rates were calculated from changes in dissolved oxygen concentrations relative to the initial oxygen concentrations after *in situ* incubation of samples under light and dark conditions, respectively. GPP_{pk} rates were then calculated following the mass balance equation $GPP_{pk} = NEP_{pk} + R_{pk}$. Metabolism experiments failed and yielded

255   negative R_{pk} rates at low tide day during winter only. Here, $NEP_{pk} > 1$ represents a net planktonic autotrophy and $NEP_{pk} < 1$ represents a net planktonic heterotrophy. In order to convert planktonic metabolism rates from oxygen to carbon, we used an average photosynthetic quotient (PQ = 1.3) from similar coastal systems and a typical respiratory quotient (RQ = 1.0) as used in most studies (Caffrey, 2004; Gazeau et al., 2004; Laws, 1991; Wielgat-Rychert et al., 2017). Results were expressed in volumetric rate (µmol CO_2 L^{-1} h^{-1}). At each HT, the integrated NEP_{pk} rate (mmol CO_2 m^{-2} h^{-1}) was estimated from the

260   volumetric NEP_{pk} rate and the water height above the marsh to compare planktonic aquatic metabolism with total aquatic metabolism and water-air CO_2 fluxes (see below). For each 24-h cycle, a daily C balance (g C m^{-2} d^{-1}) was obtained by considering the four NEP_{pk} rates measured every 6 h, at LT and HT successively.

2.5. Data processing

265   In this study, dissolved inorganic carbon (DIC; Table 1) concentrations were calculated from measured salinity, temperature, DSi, DIP, water pCO_2 and TA, using the carbonic acid constant from Mehrbach et al. (1973) as modified by Dickson and Millero (1987), the $KHSO_4$ constant from Dickson (1990) and the borate acidity constant from Lee et al. (2010). The CO_2 system calculation program (CO_2SYS, version 2.1.) performed these calculations (Lewis and Wallace, 1998). Over the 24-h cycles, water-air CO_2 fluxes and total aquatic metabolism were simultaneously estimated at each HT

270   during the highest immersion levels with limited horizontal exchanges (for 2 h over C1-winter and C3-summer and for 3.5 h over C2-spring and C4-fall).

2.5.1. Water-air CO$_2$ fluxes (FCO$_2$)

Diffusive CO$_2$ fluxes (FCO$_2$, mmol m^{-2} h^{-1}) at the water-air interface were estimated during HT periods as follows (Mayen et al., 2023):

$$FCO_2 = k\alpha(\text{water } pCO_2 - \text{air } pCO_2) \tag{1}$$

where k (cm h^{-1}) is the CO$_2$ gas transfer velocity and α (mol kg^{-1} atm^{-1}) is the CO$_2$ solubility coefficient in saltwater (Weiss, 1974). Water pCO$_2$ (ppmv) were measured by the C-sense^{TM} probe, while air pCO$_2$ (ppm) were measured by the EC station at a height of 3.15 m. FCO$_2$ > 0 (i.e. water pCO$_2$ > air pCO$_2$) indicates a CO$_2$ source from water to atmosphere and FCO$_2$ < 0 (i.e. water pCO$_2$ < air pCO$_2$) indicates an atmosphere CO$_2$ sink by the water column. We used the k-wind parametrization of Van Dam et al. (2019), which is a coefficient specific to shallow and microtidal estuaries but can be adapted to salt marsh systems (Song et al., 2023). Currently, there is no consensus on the k value parameterization in shallow coastal systems, such as salt marshes, mainly because k depends on several drivers acting at the same time: wind, current, water depth, friction at the bottom, heating and cooling. In this study, we used the k parameterization of Van Dam et al. (2019) as a function of wind speed, that was determined from concomitant pCO$_2$ and FCO$_2$ eddy covariance data in an estuarine system with characteristics very similar with our study site. The gas transfer coefficient, normalized to a Schmidt number of 600 (k_{600}) obtained from Van Dam et al. (2019), were converted to the CO$_2$ transfer velocity according to *in situ* temperature and salinity (k or k_{660}) following Jähne et al. (1987).

2.5.2. Net ecosystem production of water column (NEP$_{tot}$)

NEP$_{tot}$ was calculated by considering the changes in DIC concentrations between two discrete samplings during the highest marsh immersion levels and corrected for CaCO$_3$ production/dissolution and water-air CO$_2$ flux as follows (Cotovicz et al., 2021; Longhini et al., 2015):

$$NEP_{tot} = ((nDIC_1 - nDIC_2)\rho d) / \Delta t - ((nTA_1 - nTA_2)\rho d \times 0.5) / \Delta t - FCO_2 \tag{2}$$

where $nDIC_1$ and $nDIC_2$ are DIC concentrations (mmol kg^{-1}) normalized to salinity between two samplings, nTA_1 and nTA_2 are TA concentrations (mmol kg^{-1}) normalized to salinity between two samplings, ρ is the water density (kg m^{-3}), d is the water depth (m), Δt is the time interval (h) between the two discrete samplings and FCO$_2$ is the water-air CO$_2$ flux (mmol m^{-2} h^{-1}). NEP$_{tot}$ estimated total aquatic metabolism (the whole aquatic community and benthic processes), whereas NEP$_{pk}$ studied planktonic aquatic metabolism only (< 100 µm).

2.6. Data analysis and statistical tools

For each 24-h cycle, a linear regression between TA and DIC normalized to a constant salinity (nTA and nDIC, respectively) was performed to highlight dominant biogeochemical processes affecting DIC and TA (Borges et al., 2003; Saderne et al., 2019). Over the 24-h cycles, large salinity ranges were measured and DIC and TA were normalised according

to Friis et al. (2003) with a daily salinity mean (25.0, 36.7, 36.0 and 33.2 in C1-winter, C2-spring, C3-summer and C4-fall, respectively) to limit evaporation and dilution processes on these parameters (Koné and Borges, 2008; Saderne et al., 2019).

The data from the discrete samplings over the year were not normally distributed (Shapiro-Wilk tests, $p < 0.05$). Thus, non-parametric comparisons, including the Mann-Whitney and Kruskal-Wallis tests, were carried out with 0.05 level of significance. A Dunn test was used to perform a post-hoc multiple comparison of the Kruskal-Wallis test to detect significant differences between groups. Multiple factor variance analyses were performed using all discrete sampling data over the year ($n = 59$) to test the contribution of seasonal, diurnal and tidal factors on water biogeochemical parameters. Seasonal factor assesses variability between the 24-h cycles, tidal factor assesses variability between high tide and low tide and diurnal factor assesses variability between daytime and night-time. Parameters that did not respect a normal distribution were transformed into $\log_{10}(x)$ or $\log_{10}(x+1)$ for variance analysis. To assess the influence of biological drivers on water pCO_2, we performed a pairwise Spearman's correlation analysis from hourly water samples during the four 24-h cycles ($n = 59$).

3. Results

3.1. Meteorological and environmental settings

Air temperature (Ta) averaged over our 24-h cycles were within the standard deviations of 3-year seasonal means (continuous measurements during three full seasons), although C1-winter was significantly warmer (+2.1°C) and C4-fall was significantly colder (-2.4°C) than the seasonal reference period (Mann-Whitney tests, $p < 0.05$) (Table S1). C3-summer was the warmest period, whereas C1-winter and C4-fall were the coldest periods with similar thermal conditions. The full seasonal range in solar radiation was captured over the 24-h cycles; however, C1-winter was brighter and C4-fall was less bright than the seasonal reference period (Table S1). C2-spring and C3-summer were the brightest periods with similar daytime PAR values. On average, in C2-spring and C3-summer, wind speeds were similar to the seasonal reference periods whereas in C1-winter, wind speeds were lower (Table S1). In C1-winter, winds came from northeast while in C2-spring and C3-summer, higher wind rotations were recorded with mainly westerly winds. The driest and wettest periods were C2-spring and C4-fall, respectively, associated with the lowest and the highest 7-day cumulative rainfall. Globally, the 24-h cycles can be characterized with different meteorological conditions based on light, temperature and humidity.

In 2021, salinity of coastal waters was measured bimonthly at a marine station within the continental shelf (Filiere W; Fig. 1-A) and ranged from 27.6 (winter) to 34.8 (summer). At the salt marsh, salinity measured at high tide was very similar to coastal waters, while salinity measured at low tide showed stronger seasonal variations, ranging from 21.4 (C1-winter) to 44.2 (C3-summer; Fig. 2). The daily duration of high tides (i.e. marsh immersion) was 8 h d^{-1} over C1-winter and C3-summer (lowest tidal ranges) and 10 h d^{-1} over C2-spring and C4-fall (highest tidal ranges; Fig. 2). Water temperatures (Tw) varied between 6.4°C (C4-fall) and 28.1°C (C3-summer). Similarly, large amplitudes of DO and water pCO_2 were measured over the 24-h cycles, with DO-sat. ranging between 13% (C3-summer) and 187% (C2-spring) and pCO_2 ranging between 83 ppmv (C3-summer) and 1461 ppmv (C1-winter). For each variable, these extreme values were measured at low tide in channel waters between the day (LT/Day) and the night (LT/Night; Fig. 2).

11

3.2. Temporal variations of water pCO₂ and water-air CO₂ fluxes

For each 24-h cycle, the average water pCO_2 value was within the standard deviation of the 5-day seasonal mean computed from continuous measurements done at each season right before the 24-h cycle samplings (Table S2). On average, at seasonal scale, water pCO_2 values were higher than air pCO_2 values (water oversaturation) over C1-winter and C4-fall (669 ± 327 and 422 ± 73 ppmv, respectively) and the opposite (water pCO_2 < air pCO_2; water undersaturation) was recorded over C2-spring and C3-summer (239 ± 105 and 271 ± 182 ppmv, respectively). Water pCO_2 differed significantly between each 24-h cycle (Kruskal-Wallis test, $p < 0.0001$), except between C2-spring and C3-summer (Dunn's test, $p = 0.16$).
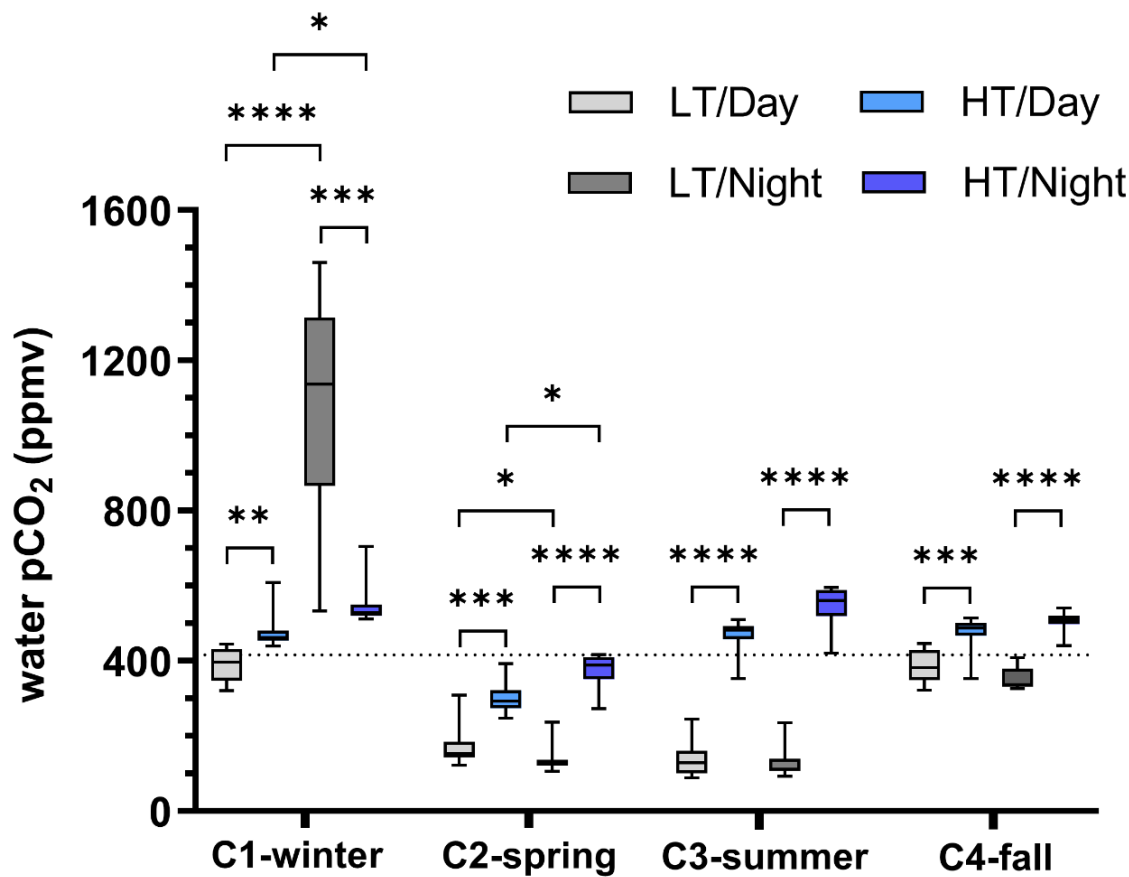

Fig. 3. Boxplot distribution of water pCO₂ variations measured every 10-min. at diurnal/tidal scales during each seasonal 24-h cycle (n = 36 for each boxplot). Horizontal dotted line corresponds to air pCO₂ measured by the EC station and averaged over the four 24-h cycles (416 ppm). Asterisks designate significant differences at diurnal/tidal scales (**** p < 0.0001, *** p < 0.001, ** p < 0.01, * p < 0.05; absence of asterisk means no significant difference p > 0.05). LT/Day: low tide day; HT/Day: high tide day; LT/Night: low tide night; HT/Night: high tide night. Low tide and high tide periods were separated into Hw (water height) = 0.50 m and 0.50 < Hw < 2.50 m, respectively, in the sampling channel (see Fig. 2 for further details).

Water pCO$_2$ varied strongly within each 24-h cycle according to diurnal and tidal scales with, in general, (1) daytime pCO$_2$ decreases and night-time pCO$_2$ increases and (2) lower pCO$_2$ values at low tide than at high tide whatever the diurnal scale (except in winter; Fig. 2). Over C1-winter, the largest diurnal/tidal water pCO$_2$ variation was recorded ranging from 321 ppmv at LT/Day (CO$_2$ undersaturation period) to 1461 ppmv at LT/Night (CO$_2$ oversaturation period) (Fig. 3). Over C2-spring and C3-summer at low tide (LT/Day and LT/Night), water was strongly undersaturated in CO$_2$ whereas at high tide (HT/Day and HT/Night), water was slightly undersaturated in CO$_2$ in C2-spring and slightly oversaturated in CO$_2$ in C3-summer (Fig. 3). Finally, over C4-fall, the lowest diurnal/tidal variation was recorded (from 311 to 541 ppmv) associated with slight water CO$_2$ undersaturation at low tide and slight water CO$_2$ oversaturation at high tide (Fig. 3). For each 24-h cycle, significant differences in water pCO$_2$ were highlighted at diurnal/tidal scales (Kruskal-Wallis tests, $p < 0.0001$; Fig. 3), except between LT/Day and LT/Night and between HT/Day and HT/Night over both C3-summer (Dunn's tests, $p = 0.90$ and $p = 0.60$, respectively) and C4-fall (Dunn's tests, $p = 0.21$ and $p = 0.07$, respectively). For all pCO$_2$ values measured over the year (n = 570), the variance analysis highlighted a significant effect of seasonal (F = 194.6, $p < 0.0001$) and tidal (F = 243.6, $p < 0.0001$) factors on $\log_{10}(pCO_2)$ but no significant diurnal effect (F = 0.9, $p = 0.33$). During high tide periods, mean water-air FCO$_2$ from water pCO$_2$ were estimated to be 0.25 ± 0.16 (source), -0.26 ± 0.18 (sink), 0.36 ± 0.14 (source) and 0.47 ± 0.10 (source) mmol m^{-2} h^{-1} over C1-winter, C2-spring, C3-summer and C4-fall, respectively (Table 2). Significant seasonal variations in water-air FCO$_2$ were recorded between the 24-h cycles (Kruskal-Wallis, $p < 0.0001$).

3.3. Planktonic biomass, abundance and metabolism

Chl*a* concentration medians increased from C1-winter to C4-fall (Table 1). Over C1-winter, Chl*a* varied independently of water height whereas during the other 24-h cycles, higher Chl*a* concentrations were recorded at low tide than at high tide (Fig. 4 and Fig. S1). Over the 24-h cycles, microphytoplankton (> 20 µm) was composed mainly of pennate diatoms (except in C3-summer when a dinoflagellate bloom occurred) with an abundance increase from high to low tide over both C2-spring and C3-summer (Fig. 4-A). For smaller cells (< 20 µm), nanophytoplankton was more abundant at low tide than at high tide (except over C1-winter), while picophytoplankton was more abundant at low tide during C2-spring only (Fig. 4-B). Higher planktonic bacteria abundances were also recorded at low tide with highest and lowest tidal variations occurring during C2-spring/C3-summer and C1-winter/C4-fall, respectively (Fig. 4-C).

Over the 24-h cycles, NEP$_{pk}$ rates varied strongly according to light (daytime *vs.* night-time) and water height (low tide *vs.* high tide). Generally, the sampled planktonic communities were autotrophic (NEP$_{pk}$ > 0) during daytime and heterotrophic (NEP$_{pk}$ < 0) during night-time irrespective of water height (Fig. 5-A). However, a stronger planktonic metabolism (production and respiration) was systematically recorded at low tide than at high tide (Fig. 5-A,B). At low tide, daytime NEP$_{pk}$ rates ranged from 0.54 ± 0.10 (C4-LT/Day) to 5.24 ± 0.39 µmol L^{-1} h^{-1} (C2-LT/Day), while night-time NEP$_{pk}$ rates ranged from -0.92 ± 0.64 (C1-LT/Night) to -2.15 ± 0.35 µmol L^{-1} h^{-1} (C3-LT/Night). The highest R$_{pk}$ and GPP$_{pk}$ rates were recorded at low tide, especially during C2-LT/Day and C3-LT/Day (Fig. 5-B,C). Across all measured rates (n = 16),

13

390   R_{pk} were significantly related to bacteria abundance ($R^2 = 0.50$, $p < 0.05$) but not to Chl$a$ concentrations ($p = 0.14$; data not shown).

     At each high tide, planktonic aquatic metabolism (NEP_{pk}) was compared simultaneously with total aquatic metabolism (NEP_{tot}) (Table 2). Planktonic community was net autotrophic at C1-HT/Day and C3-HT/Day (NEP_{pk} = 0.89 and 0.43 mmol m^{-2} h^{-1}, respectively), while total aquatic community was net autotrophic at C2-HT/Day only (NEP_{tot} = 0.91 mmol m^{-2} h^{-1}).

395   Generally, NEP_{pk} rates were weaker than NEP_{tot} rates and similar metabolic status (autotrophy *vs.* heterotrophy) were recorded except over C1-C2-C3-HT/Day (Table 2).

Table 1. Medians (in bold) and associated ranges (min – max in brackets) of water biogeochemical parameters measured from hourly sampling during the four seasonal 24-h cycles (n = 13 over C1-winter, n = 15 over C2-spring and C3-summer and n = 16 over C4-fall; see Fig. S1 to view data from the hourly samplings).

|	C1-winter	C2-spring	C3-summer	C4-fall
Chlorophyll a	**2.6**	**4.2**	**7.0**	**11.4**
Chl$a$ (µg L^{-1})	(1.2 – 5.0)	(1.4 – 25)	(1.3 – 17)	(1.0 – 29)
Dissolved Inorganic Carbon	**2799**	**2173**	**2056**	**2584**
DIC (µmol kg^{-1})	(2354 – 3963)	(2053 – 2530)	(1587 – 2175)	(2206 – 2762)
Total Alkalinity	**3076**	**2757**	**2385**	**2804**
TA (µmol kg^{-1})	(2508 – 4016)	(2379 – 2947)	(2228 – 2812)	(2351 – 3047)
Dissolved Organic Carbon	**288**	**519**	**358**	**289**
DOC (µM)	(124.0 – 596)	(161.9 – 1040)	(97.4 – 1010)	(93.1 – 529)
Particulate Organic Carbon	**188**	**151**	**166**	**101**
POC (µM)	(42 – 581)	(27 – 560)	(30 – 1048)	(21 – 270)
Particulate Organic Nitrogen	**16**	**17**	**28**	**15**
PON (µM)	(3.2 – 39)	(2.7 – 68)	(3.7 – 131)	(3.8 – 36)
Nitrate + Nitrite	**19.0**	**1.0**	**0.60**	**1.5**
NO_3^-_NO_2^- (µM)	(8.4 – 31)	(0.37 – 1.7)	(0.20 – 0.80)	(0.35 – 5.3)
Ammonium	**33**	**2.9**	**2.1**	**3.3**
NH_4^+ (µM)	(2.5 – 60)	(0.51 – 7.7)	(0.59 – 4.0)	(1.59 – 6.6)
Phosphate	**1.1**	**0.19**	**0.75**	**0.25**
DIP (µM)	(0.56 – 2.3)	(0.05 – 0.88)	(0.12 – 1.73)	(0.11 – 0.39)
Silicate	**27**	**14.4**	**23**	**7.2**
DSi (µM)	(21 – 94)	(2.2 – 27)	(8.4 – 40)	(5.2 – 12.5)
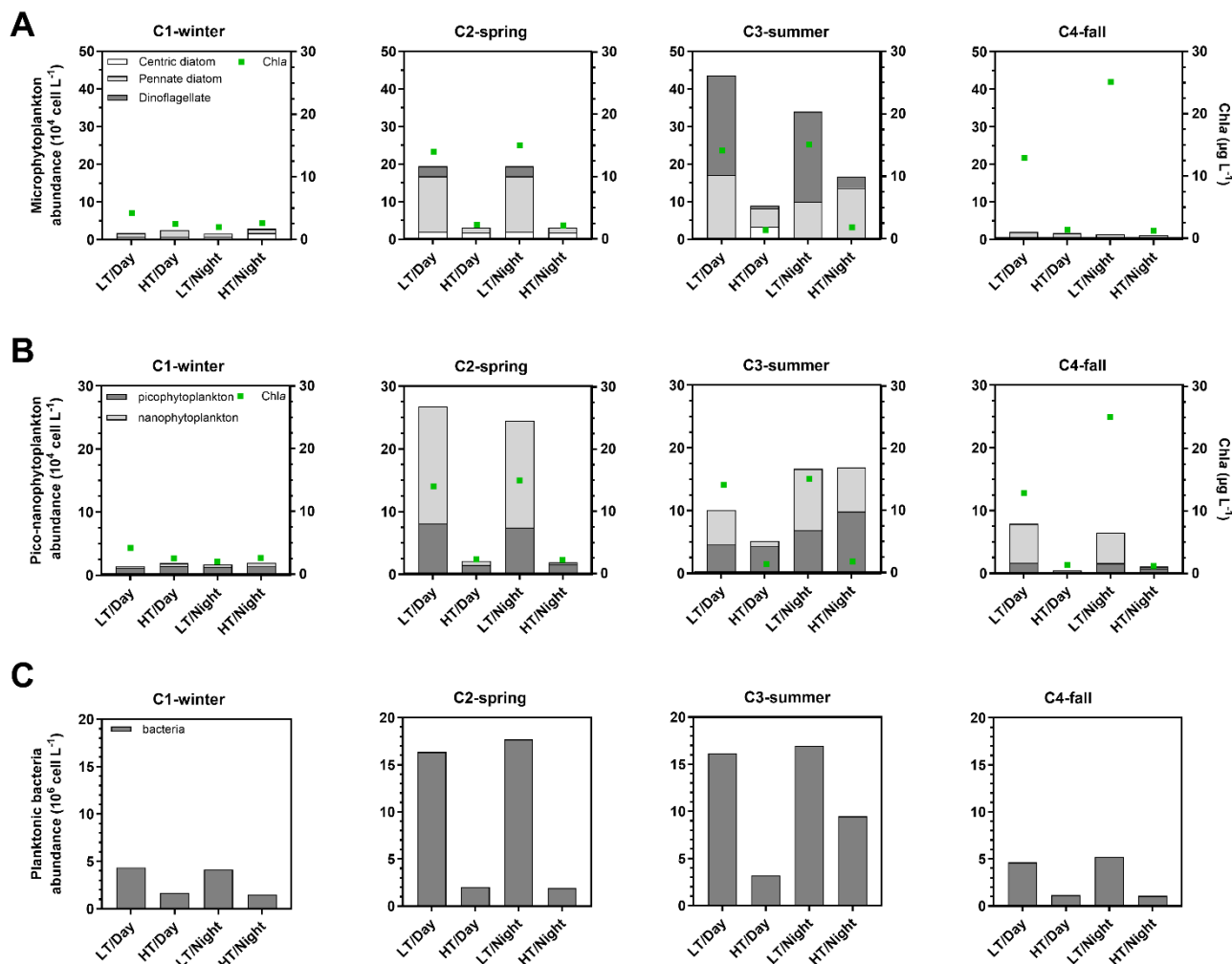
Fig. 4. Abundance of microphytoplankton (A; 10^4 cell L^{-1}), pico-nanophytoplankton (B, 10^4 cell L^{-1}) and total planktonic bacteria (10^6 cell L^{-1}) sampled at diurnal/tidal scales during each seasonal 24-h cycle simultaneously to measurements of planktonic aquatic metabolism (NEP$_{pk}$). Contrary to the water biogeochemical parameters sampled every one or two hours over the 24-h cycles, planktonic communities were sampled every 6 hours once of each period of LT/Day, HT/Day, LT/Night and HT/Night (n = 4). The Chl$a$ concentration medians associated to each period (LT/Day, HT/Day, LT/Night and HT/Night) was added in green. Microphytoplankton was separated into centric diatoms, pennate diatoms and dinoflagellates. LT/Day: low tide day; HT/Day: high tide day; LT/Night: low tide night; HT/Night: high tide night.
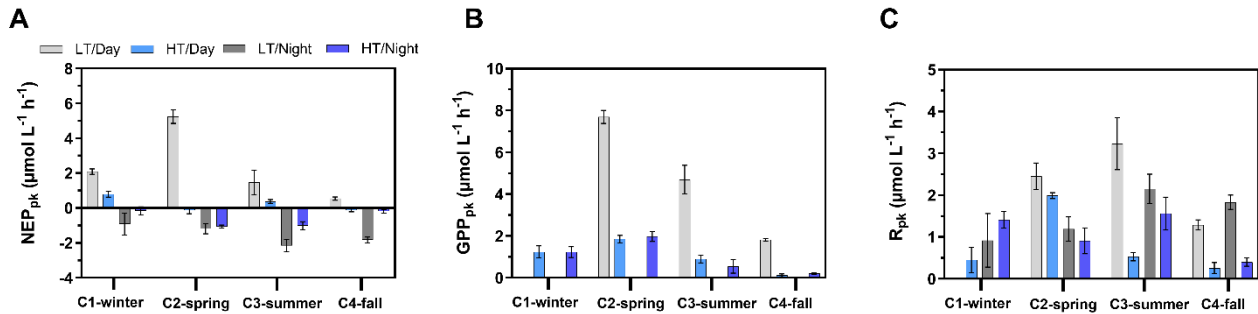
Fig. 5. Planktonic aquatic metabolism and associated standard errors measured at diurnal/tidal scales during each seasonal 24-h cycle: (A) planktonic net ecosystem production (NEP_{pk}), (B) planktonic respiration (R_{pk}) and (C) planktonic gross primary production (GPP_{pk}). All metabolic rates are expressed in µmol CO_2 L^{-1} h^{-1}. $NEP_{pk} > 0$ corresponds to a planktonic autotrophy (CO_2 sink in water) and $NEP_{pk} < 0$ corresponds to a planktonic heterotrophy (CO_2 source in water). LT/Day: low tide day; HT/Day: high tide day; LT/Night: low tide night; HT/Night: high tide night.
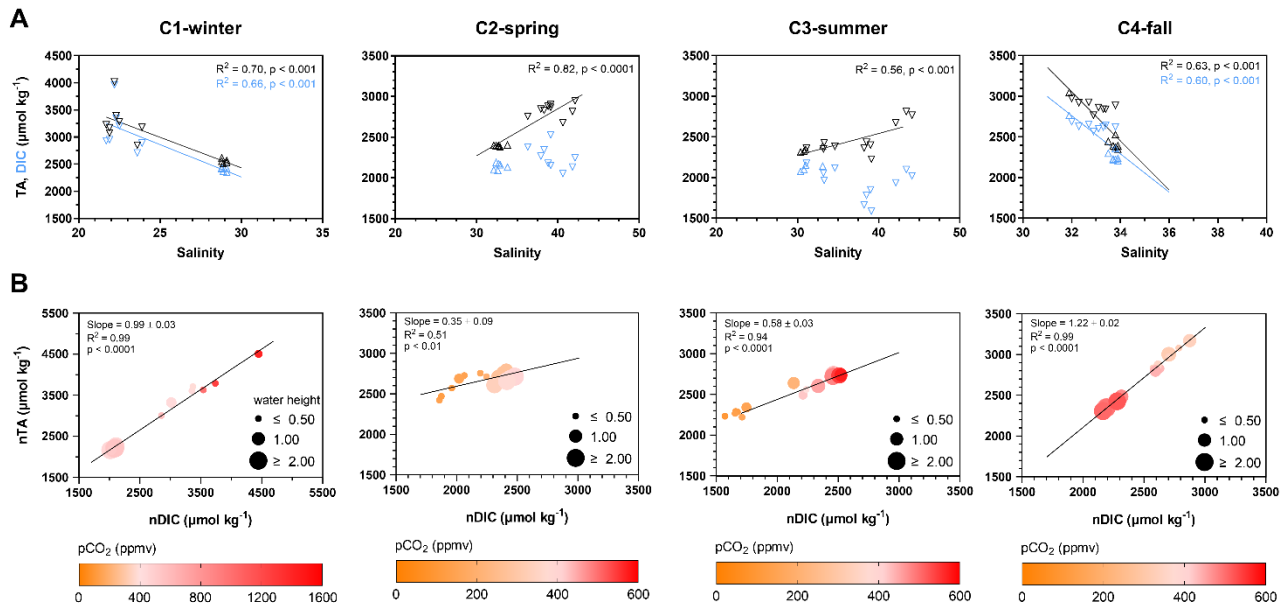

Fig. 6. (A) Cross correlation plots of TA (black triangles) and DIC (blue triangles) concentrations *versus* salinity values for each seasonal 24-h cycle. Downward triangles correspond to low tide (LT) and upward triangles correspond to high tide (HT). Salinity values at high tide were similar between the 24-h cycles, but salinity values at low tide strongly differed between the 24-h cycles. (B) Significant linear regressions between normalized TA (nTA) *versus* normalized DIC (nDIC) for each seasonal 24-h cycle. nTA and nDIC data were calculated from Friis et al. (2003) with a mean salinity value for all samples (25.0, 36.7, 36.0 and 33.2 at C1-winter, C2-spring, C3-summer and C4-fall, respectively; see M&M section). Water pCO_2 levels (ppmv) are represented by a colour gradient whereas water heights (m) are represented by a size gradient. Only the significant linear regressions ($p < 0.05$) are showed. See Fig. S1 to view data from the hourly samplings.

Table 2. Diurnal comparison of planktonic aquatic metabolism (NEP$_{pk}$) and total aquatic metabolism (NEP$_{tot}$) during each high tide (HT/Day *versus* HT/Night). Simultaneously, water pCO$_2$ measured by the C-Sense^{TM} probe, water-air CO$_2$ fluxes (FCO$_2$) estimated from water pCO$_2$ and net ecosystem CO$_2$ exchanges (NEE) measured by EC were recorded (means and SD in bold, ranges in brackets) and related to aquatic metabolism. Positive and negative NEP$_{pk}$ and NEP$_{tot}$ rates correspond to an autotrophy and a heterotrophy in water, respectively, whereas positive and negative FCO$_2$ and NEE fluxes correspond to a source and a sink of CO$_2$, respectively. Wind directions measured by EC are ESE over C1-winter, WNW and NNW over C2-spring and WNW over C3-summer. The CO$_2$ transfer velocity (k_{660}) obtained from Van Dam et al. (2019) were recorded. n.a.: not available.

		Planktonic aquatic metabolism	Total aquatic metabolism	Water CO$_2$ partial pressure	CO$_2$ transfer velocity	Water-air CO$_2$ fluxes	Net ecosystem CO$_2$ exchanges
		NEP$_{pk}$ (mmol m^{-2} h^{-1})	NEP$_{tot}$ (mmol m^{-2} h^{-1})	pCO$_2$ (ppmv)	k_{660} (cm h^{-1})	FCO$_2$ (mmol m^{-2} h^{-1})	NEE (mmol m^{-2} h^{-1})
C1-winter	HT/Day	**0.89**	**-29.02**	**478 ± 45** (439 – 613)	**4.89 ± 0.38** (4.44 – 5.44)	**0.08 ± 0.02** (0.05 – 0.09)	**0.28 ± 2.21** (-6.80 – 3.42)
	HT/Night	**-0.23**	**-11.65**	**546 ± 51** (510 – 776)	**7.39 ± 0.51** (6.50 – 7.74)	**0.38 ± 0.05** (0.33 – 0.46)	**-3.22 ± 1.72** (-8.86 – -0.40)
C2-spring	HT/Day	**-0.20**	**0.91**	**302 ± 37** (247 – 393)	**9.27 ± 2.06** (5.89 – 9.93)	**-0.40 ± 0.08** (-0.52 – -0.29)	**-6.27 ± 0.49** (-6.98 – -5.29)
	HT/Night	**-1.77**	**-27.71**	**377 ± 38** (272 – 416)	**7.55 ± 1.60** (5.99 – 9.66)	**-0.14 ± 0.12** (-0.34 – -0.03)	**0.88 ± 2.31** (-4.25 – 7.96)
C3-summer	HT/Day	**0.43**	**-5.59**	**469 ± 41** (335 – 514)	**10.04 ± 0.74** (9.25 – 10.85)	**0.23 ± 0.01** (0.22 – 0.24)	**-4.15 ± 2.63** (-7.56 – -1.38)
	HT/Night	**-0.73**	**-47.02**	**546 ± 49** (412 – 597)	**9.64 ± 0.22** (9.43 – 9.94)	**0.48 ± 0.07** (0.40 – 0.52)	**-1.71 ± 1.58** (-4.46 – 0.11)
C4-fall	HT/Day	**-0.18**	**-3.77**	**472 ± 42** (353 – 514)	**9.83 ± 0.74** (8.62 – 10.85)	**0.44 ± 0.05** (0.37 – 0.49)	n.a.
	HT/Night	**-0.27**	**-22.21**	**507 ± 23** (441 – 541)	**8.54 ± 2.39** (4.81 – 10.76)	**0.49 ± 0.13** (0.30 – 0.62)	n.a.

17

3.4. Carbon and nutrient temporal variations

DIC and TA concentrations followed similar seasonal and tidal variations with decreases from C1-winter to C3-summer (Table 1) and increases from high to low tide (Fig. 6-A and Fig. S1). Over the 24-h cycles, DIC and TA varied strongly according to salinity (i.e. tidal scale), especially during C1-winter, where the highest DIC and TA concentrations were recorded at low tide night (Fig. 6-A). Moreover, a significant linear relationship between salinity-normalized TA (nTA) and salinity-normalized DIC (nDIC) was found over each 24-h cycle with slopes ranging from 0.35 in C2-spring ($R^2 = 0.51$, n = 12, $p < 0.01$) to 1.22 in C4-fall ($R^2 = 0.99$, n = 16, $p < 0.001$; Fig. 6-B).

Organic carbon also varied significantly at seasonal scale (Kruskal-Wallis tests, $p < 0.05$) with the highest POC and DOC concentrations recorded over C1-winter and C2-spring, respectively (Table 1). At tidal scale, the highest concentrations were recorded at low tide and the lowest at high tide (Fig. 7-A,B and Fig. S1). For example, during C2-spring, POC and DOC medians ranged from 40 to 231 µM and from 199 to 873 µM, respectively, from high to low tide. Systematically, large increases in carbon were recorded from high to low tide with (1) DIC increases predominating over C1-winter and C4-fall and (2) DOC increases predominating over C2-spring and C3-summer (Fig. A,B). Over all 24-h cycles, POC:PON ratios at low tide varied between 6 and 8 (except in C1-winter when the highest POC:PON ratios were recorded; Fig. 7-C). A large seasonal amplitude of POC:Chl$a$ ratios was recorded with highest and lowest ratios recorded at low tide over C1-winter (> 700 mg mg^{-1}) and C4-fall (< 200 mg mg^{-1}), respectively (Fig. 7-D). Over C2-spring, lower POC:Chl$a$ ratios were recorded at low tide than at high tide whereas over C3-summer, the opposite was observed.

Nutrients also varied significantly between seasons (Kruskal-Wallis tests, $p < 0.05$), with a strong decrease in NO_3^-_NO_2^- and NH_4^+ concentrations from C1-winter to C2-spring. DIP and DSi concentrations also decreased from C1-winter to C2-spring before increasing towards C3-summer (Table 1). On a shorter timescale (hourly sampling; Fig. S1), significantly higher concentrations of NH_4^+, DSi and DIP were recorded at low tide than at high tide (Mann-Whitney tests, $p < 0.05$) whatever the diurnal scale, especially (1) over C1-winter for NH_4^+ (Fig. 7-F), (2) over C2-spring and C3-summer for DSi (Fig. 7-G) and (3) over C1-winter and C3-summer for DIP (Fig. 7-H) where the greatest amplitudes were recorded. Conversely, NO_3^-_NO_2^- concentrations were significantly lower at low tide than at high tide (Mann-Whitney tests, $p < 0.05$), especially over C1-winter (Fig. 7-E).
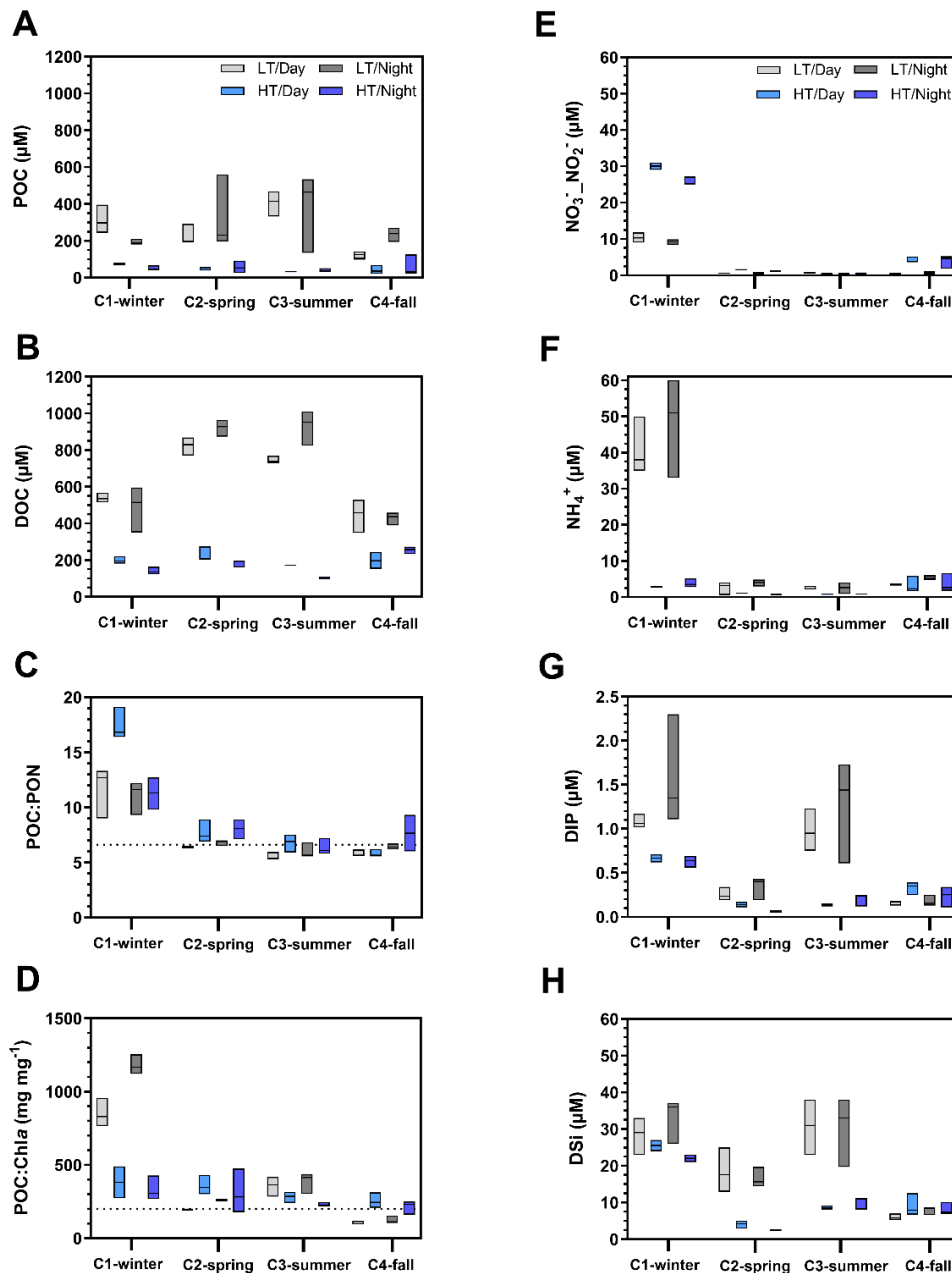
Fig. 7. Boxplot distribution of water biogeochemical parameters measured from hourly sampling during the seasonal 24-h cycles: (A) POC, (B) DOC, (c) POC:PON molar ratio, (d) POC:Chl*a* mass ratio and (E, F, G, H) nutrients. The horizontal dotted line in Fig. 7-C corresponds to the Redfield ratio (i.e. theorical molar ratio for plankton; POC:PON = 6.6 µmol µmol^{-1}) (Redfield, 1958). The horizontal dotted line in Fig. 7-D characterizes particulate organic matter either as autotrophic (POC:Chl*a* < 200 mg mg^{-1}, dominance of "fresh" living phytoplankton) or heterotrophic (POC:Chl*a* > 200 mg mg^{-1}, dominance of detrital organic material) (Savoye et al., 2003). LT/Day: low tide day; HT/Day: high tide day; LT/Night: low tide night; HT/Night: high tide night. Low tide and high tide periods were separated into Hw = 0.50 m and 0.50 < Hw < 2.50 m, respectively, in the sampling channel. See Fig. S1 to view data from the hourly samplings.

19

3.5. Correlations and multiple factor variance analysis

In all discrete samplings over the year (n = 59), DOC and Chl*a* displayed strong negative correlations with water pCO_2, whereas DIC and NO_3^-_NO_2^- showed weak positive correlations with water pCO_2 (Table 3). Organic carbon (POC and DOC) was positively correlated with Chl*a*, whereas NO_3^-_NO_2^- was negatively correlated with Chl*a*. Increases in NH_4^+ from high to low tide were strongly and positively correlated with TA and DIC (Table 3), especially over the C1-winter (Fig. S1). Variance analyses of dissolved inorganic matter showed that TA, NH_4^+ and DSi were much more explained by tides than seasons, whereas the opposite was found for NO_3^-_NO_2^- and DIC (Table S3). Regarding dissolved organic matter, DOC was mainly controlled by tides (weak seasonal influence) whereas for particulate organic matter, POC was solely controlled by tidal factor (Table S3). Diurnal factor did not significantly explain variance in measured biogeochemical parameters (except for DIP) but significantly affected the carbonate system parameters (DIC, TA, and pCO_2) over C1-winter only.

Table 3. Spearman's rank correlations of water biogeochemical parameters recorded from hourly water samples during the four 24-h cycles (n = 59). Asterisks designate significant correlations (* $p < 0.001$, ** $p < 0.01$, * $p < 0.05$, n.a. $p > 0.05$).**

	Chl*a*	DIC	TA	NO_3^-_NO_2^-	NH_4^+	DIP	DSi	DOC	POC	PON
pCO_2	-0.61***	0.51***	n.a.	0.59***	n.a.	n.a.	n.a.	-0.68***	-0.56***	-0.64***
Chl*a*		n.a.	0.45***	-0.50***	0.32*	n.a.	0.25*	0.69***	0.78***	0.84***
DIC			0.73***	0.38***	0.67***	n.a.	n.a.	n.a.	n.a.	n.a.
TA				n.a.	0.87***	0.27*	0.37**	0.49***	0.57***	0.42**
NO_3^-_NO_2^-					0.25*	0.37**	n.a.	-0.39**	n.a.	-0.43**
NH_4^+						0.47***	0.46***	0.40**	0.49***	0.35**
DIP							0.87***	0.36*	0.50***	0.37**
DSi								0.46***	0.68***	0.50***
DOC									0.80***	0.85***
POC										0.92***

3.6. Net ecosystem CO$_2$ exchanges (NEE) and daily C balances

Significant seasonal variations in measured NEE were highlighted between each 24-cycle (Kruskal-Wallis test, p < 0.001). On average, the highest and lowest marsh atmospheric CO$_2$ sinks within the footprint were measured over C3-summer (-2.70 ± 5.00 µmol m^{-2} s^{-1}) and C1-winter (-1.37 ± 2.66 µmol m^{-2} s^{-1}), respectively (Fig. 2). Over the 24-h cycles, the highest CO$_2$ uptake and CO$_2$ emission were recorded at low tides during daytime and night-time, respectively, associated with a major influence of marsh metabolism at the soil-air interface (i.e. measured NEE = estimated NEE$_{marsh}$; Fig. 2). During each high tide period, immersion strongly disrupted NEE though, in general, no change in the marsh CO$_2$ sink/source status was noted (Fig. 2). For instance, at HT/Day, significant differences were recorded between measured NEE and estimated NEE$_{marsh}$ over C1-winter and C2-spring (Wilcoxon tests, p < 0.05), where tides decreased net marsh CO$_2$ uptake by 80% and 68%, respectively (Fig. 2). However, no significant difference between measured NEE and estimated NEE$_{marsh}$ was recorded over C3-summer at HT/Day (Wilcoxon test, p = 0.41; NEE = NEE$_{marsh}$) though water CO$_2$ oversaturation was measured at this time (553 ± 40 ppmv; Fig. 2). At HT/Night, lower marsh CO$_2$ emissions (NEE) were measured in comparison with estimated NEE$_{marsh}$ (Wilcoxon tests, p < 0.05) even inducing a switch from source to sink over C1-winter, though water CO$_2$ oversaturation was measured over the same time (533 ± 12 ppmv).

Over the 24-h cycles, daily C balances of planktonic aquatic metabolism (NEP$_{pk}$) ranged from 0.25 (C2-spring; autotrophy) to -0.11 g m^{-2} d^{-1} (C4-fall; heterotrophy), while daily C balances of the whole marsh within the footprint (NEE) ranged from -1.43 (C1-winter; C sink) to -2.82 g m^{-2} d^{-1} (C3-summer; C sink) (Table 4). Daily C balances from estimated NEE$_{marsh}$, considering only the marsh metabolism at the soil-air interface, ranged from -1.64 (C1-winter) to -3.32 g C m^{-2} d^{-1} (C2-spring). The highest GPP$_{marsh}$ rates were recorded over C2-spring and those of R$_{marsh}$ over C3-summer. At emersion, a significant proportion of the marsh primary production (GPP$_{marsh}$) was respired and released as atmospheric CO$_2$ (R$_{marsh}$) over the 24-h cycles (R$_{marsh}$:GPP$_{marsh}$ of 26%, 33% and 42% over C1-winter, C2-spring and C3-summer, respectively; Table 4).

Table 4. Daily C balances (g C m^{-2} d^{-1}) of NEP$_{pk}$ rates (planktonic metabolism), NEE fluxes (marsh atmospheric CO$_2$ exchanges) and NEE$_{marsh}$, GPP$_{marsh}$ and R$_{marsh}$ fluxes (marsh metabolic fluxes at the benthic interface) during the four seasonal 24-h cycles. For NEP$_{pk}$ rates, positive C balances correspond to a planktonic autotrophy (net C sink in water) and negative C balances correspond to a planktonic heterotrophy (net C source in water). For marsh atmospheric CO$_2$ exchanges with immersion (NEE) and without immersion (NEE$_{marsh}$), negative C balances correspond to an atmospheric C uptake by the marsh. n.a.: not available.

	NEP$_{pk}$ (g C m^{-2} d^{-1})	NEE (g C m^{-2} d^{-1})	NEE$_{marsh}$ (g C m^{-2} d^{-1})	GPP$_{marsh}$ (g C m^{-2} d^{-1})	R$_{marsh}$ (g C m^{-2} d^{-1})
C1-winter	0.07	-1.43	-1.64	-2.22	0.58
C2-spring	0.25	-2.56	-3.32	-4.96	1.64
C3-summer	-0.06	-2.82	-2.62	-4.49	1.87
C4-fall	-0.11	n.a.	n.a.	n.a.	n.a.

4. Discussion

4.1. Temporal variations of water pCO_2 in salt marshes

The four sampling 24-h cycles done at the different seasons and tidal phases showed large and significant temporal variations in carbon biogeochemical parameters, especially in water pCO_2 (Table 5). As an illustration, we observed a maximal seasonal pCO_2 amplitude of 430 ppmv (in average between two 24-h cycles) and a maximal tidal pCO_2 variation of 1140 ppmv (between high and low tide over a 24-h cycle). During high tide both at day and night, imported coastal waters were oversaturated in CO_2 inducing atmospheric emissions during marsh immersion (except in spring; Table 2). Indeed, Mayen et al. (2023) confirmed that the coastal end-member (i.e. the continental shelf) behaved as a CO_2 source, especially in winter during the highest river water flows from the Aiguillon Bay. Thus, coastal waters imported to the studied salt marsh could degas the excess of terrestrially-derived CO_2 into the atmosphere (Fig. 8-B). In the studied salt marsh, strong water pCO_2 variations were then recorded from high to low tide due to more intense biological activity (production and respiration) at low tide in channel waters than at high tide in more buffered coastal waters as shown elsewhere by Wang et al. (2018). At low tide, in winter, the net marsh autotrophy during the day induced a small channel water pCO_2 decrease, whereas the net marsh heterotrophy during the night induced a large channel water pCO_2 increase. In contrast, during spring and summer, the intense autotrophy in channel waters induced the lowest pCO_2 values both at day and night (Fig. 2). Thus, during transient tidal phases, lateral exchanges with adjacent down- and upstream waters instantaneously produced intense channel water pCO_2 variations, leading to 1) increases during flood tides (i.e. channel filling) in response to CO_2-oversaturated coastal waters imported from the continental shelf, and 2) decreases during ebb tides (i.e. channel emptying) in response to CO_2-depleted marsh waters exported from salt ponds (Mayen et al., 2023), along with autochthonous metabolic processes (production and respiration) during these tidal periods (Fig. 8-A). Similarly, the tidal water pCO_2 variations observed over each seasonal 24-h cycle were also confirmed during the longer *in situ* measurement periods up to 5 days encompassing our 24-h samplings. These intense tidal variations confirmed that water mixing processes occurring in the channel induced large changes in carbonate chemistry mainly related to contrasted coastal and marsh end-members (Fig. 8). Our results also confirmed the substantial contribution of biological activity to water inorganic carbon pool at small timescales in salt marshes (Gong et al., 2023; Wang et al., 2016), especially water pCO_2 (Song et al., 2023; Wang et al., 2018). Other studies in coastal wetlands (seagrasses, mangroves and salt marshes) show strong tidal control in inorganic carbon but, unlike our results, the highest pCO_2 values were measured systematically at low tide irrespective of day or night (Polsenaere et al. 2022 for tidal bays, Song et al. 2023 for salt marshes and Cabral et al. 2024 for mangroves). The organic carbon mineralization in sediments followed by efflux of CO_2 oversaturated porewaters to the water column by tidal pumping generally induced large water pCO_2 increases at low tide (Borges et al., 2003; Burgos et al., 2018). Within a salt marsh-estuary coastal system (USA), water pCO_2 in summer varied from 1600 ppmv (high tide) to 12000 ppmv (low tide) (Table 5; Wang et al., 2018). Thus, horizontal exchanges of coastal waters with salt marshes strongly modify water CO_2 sink/source status due to a strong marsh metabolism (production and respiration).

Table 5. Seasonal/annual comparison of water inorganic carbon dynamics (pCO_2 in ppmv, DIC and TA in $\mu mol\ kg^{-1}$), total aquatic metabolism (NEP_{tot} in $mmol\ m^{-2}\ h^{-1}$) and water-air CO_2 fluxes (FCO_2 in $mmol\ m^{-2}\ h^{-1}$) between the Bossys perdus salt marsh (this study, France) and other similar temperate salt marsh systems in the literature. Median values were done in bold and tidal range values were done in brackets (min – max). n.a.: not available.
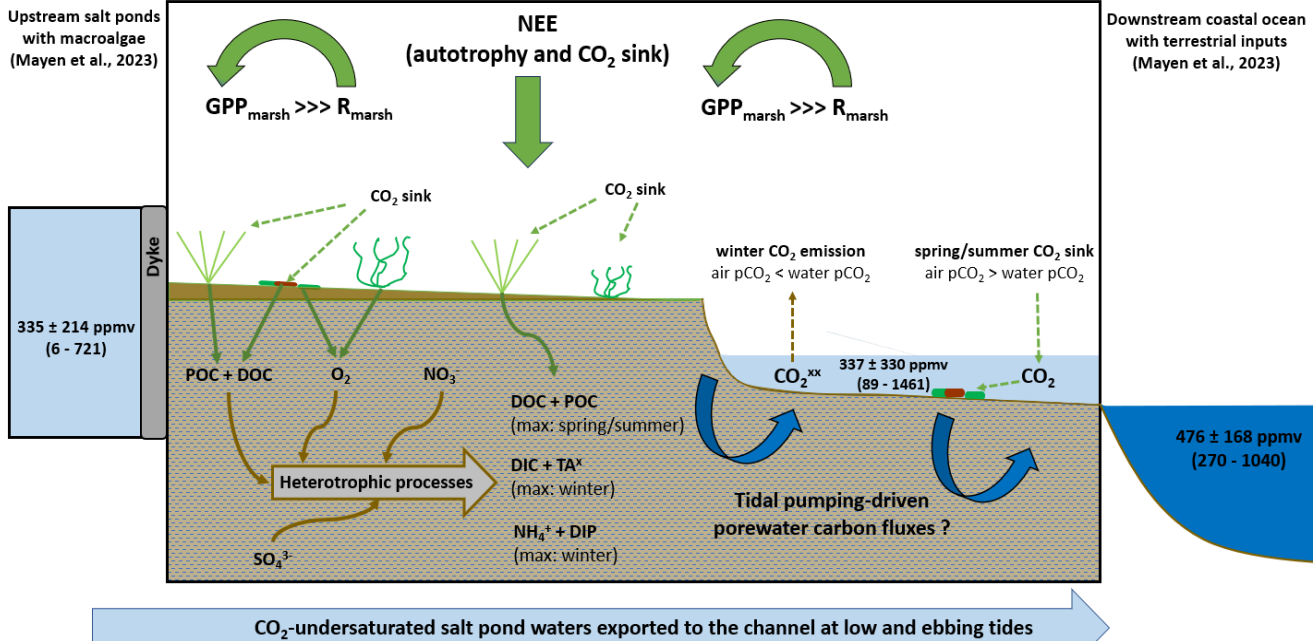
Reference		Winter	Spring	Summer	Fall	Annual
This study	Water pCO_2 (ppmv)	**525** (321 – 1461)	**221** (106 – 416)	**158** (89 – 597)	**411** (311 – 541)	**382** (89 – 1461)
	DIC ($\mu mol\ kg^{-1}$)	**2799** (2354 – 3963)	**2173** (2053 – 2530)	**2056** (1587 – 2175)	**2584** (2206 – 2762)	**2238** (1587 – 3963)
	TA ($\mu mol\ kg^{-1}$)	**3076** (2508 – 4016)	**2757** (2379 – 2947)	**2385** (2228 – 2812)	**2804** (2351 – 3047)	**2617** (2228 – 4016)
	NEP_{tot} ($mmol\ m^{-2}\ h^{-1}$)	**-20.33** (-29.02 – -11.65)	**-13.40** (-27.71 – 0.91)	**-26.31** (-47.02 – -5.59)	**-12.99** (-22.21 – -3.77)	**-16.93** (-47.02 – 0.91)
	Water-air FCO_2 ($mmol\ m^{-2}\ h^{-1}$)	**0.33** (0.05 – 0.46)	**-0.31** (-0.52 – -0.03)	**0.32** (0.22 – 0.52)	**0.45** (0.30 – 0.62)	**0.27** (-0.52 – 0.62)
Wang et al. (2018)	Water pCO_2 (ppmv)	n.a. (500 – 4000)	n.a.	n.a. (1600 – 12000)	n.a.	n.a. (500 – 12000)
	DIC ($\mu mol\ kg^{-1}$)	n.a. (1500 – 2500)	n.a.	n.a. (2250 – 4300)	n.a.	n.a. (1500 – 4300)
	NEP_{tot} ($mmol\ m^{-2}\ h^{-1}$)	-0.83	n.a.	-2.50	n.a.	-1.60
	Water-air FCO_2 ($mmol\ m^{-2}\ h^{-1}$)	0.60	n.a.	3.90	n.a.	2.05
Reithmaier et al. (2023)	DIC ($\mu mol\ kg^{-1}$)	**2158** (1610 – 3080)	**1941** (1452 – 7895)	**2052** (1450 – 4200)	**2210** (1367 – 3740)	**2065** (1367 – 7895)
	TA ($\mu mol\ kg^{-1}$)	**2262** (1634 – 3296)	**1977** (1376 – 8045)	**2083** (1578 – 4191)	**2269** (1330 – 3765)	**2104** (1330 – 8040)
Song et al. (2023)	Water-air FCO_2 ($mmol\ m^{-2}\ h^{-1}$)	n.a.	n.a.	**1.03**	**0.20**	n.a.
Gong et al. (2023)	Water-air FCO_2 ($mmol\ m^{-2}\ h^{-1}$)	n.a.	**0.53**	**0.65**	**1.10**	**0.76**
Alongi (2020)	Water-air FCO_2 ($mmol\ m^{-2}\ h^{-1}$)	n.a.	n.a.	n.a.	n.a.	**1.49**

4.2. Marsh primary producer metabolism influence on water pCO₂ and DOC

During daytime high tides, total aquatic metabolism was strongly heterotrophic ($NEP_{tot} < 0$) in winter, summer and fall indicating a weak photosynthesis of immersed marsh plants and marine phytoplankton (Table 2 and Fig. 8-B). However, during transient tidal phases from high to low tide, the large water pCO_2 decreases and DOC concentration increases, especially in spring (-54% and +77%, respectively) and summer (-71% and +85%, respectively), could be related to a strong autochthonous and allochthonous marsh primary production (Fig. 8-A). Indeed, a large part of inorganic carbon seemed to be fixed by primary producer photosynthesis (negative correlation between Chl*a* and water pCO_2) including mainly phytoplankton, benthic microalgae and macroalgae, processed by metabolic processes and then exported from/to channel waters as organic carbon (negative correlation between DOC and water pCO_2).

During the 24-h cycles, the large phytoplankton abundance increases from high to low tide, especially in spring and summer (Fig. 4), indicated a development of planktonic communities in the salt marsh under nutrient-rich conditions and low water levels. At low tide (except in winter), POC:PON ratios were close to the Redfield value (Redfield, 1958) suggesting living phytoplanktonic biomass in channel waters. Moreover, phytoplankton was highlighted as the dominant carbon source at low tide using POC stable isotope ratios ($\delta^{13}C$ of -18.3 ± 1.0‰, -17.4 ± 0.4‰ and -20.6 ± 0.9‰ in spring, summer and fall, respectively; unpublished data) according to Gearing et al. (1984). In the sampled planktonic communities, high abundances of pennate diatoms in spring and summer indicated the presence of resuspended benthic microalgae mats (microphytobenthos) whose strong autotrophic metabolism could promote the lowest water pCO_2 measured in the channel (Fig. 2) as observed elsewhere (Polsenaere et al., 2022). At low tide, these planktonic communities behaved as a CO_2 sink during daytime and as a CO_2 source during night-time (Fig. 5-A). During daytime low tide, the highest planktonic CO_2 uptake ($NEP_{pk} > 0$) was recorded in spring (high PAR and temperate Tw) through a significant autotrophic activity of pennate diatoms and nanophytoplankton, whereas the decrease in planktonic CO_2 uptake towards summer (high PAR and Tw) was concomitant to higher temperatures, promoting community respiration, and more generally, dominant heterotrophic processes (Fig. 5-B). Moreover, in summer, the dinoflagellate bloom observed at low tide, some species known to be mixotrophic or even heterotrophic (Jeong et al., 2010; Stoecker, 1999), could also be responsible for the lower planktonic CO_2 uptake in summer than in spring. Thus, planktonic metabolism at low tide could significantly influenced and reflected water pCO_2 variations, especially in spring, inducing high daytime decreases and low night-time increases (Fig. 2). Planktonic community in channel waters was an important source of DOC (positive correlation between Chl*a* and DOC), produced through extracellular releases that commonly accounting for 5-30% of their primary production (Karl et al., 1998) or through phytoplankton cell lysis which can be an important process occurring under physiological stress conditions in summer such as nutrient limitation (Van Boekel et al., 1992). In our salt marsh, pennate diatoms and nanophytoplankton as fast-growing primary producers could release high labile DOC (De Brouwer and Stal, 2001; Morelle et al., 2022) which could then be degraded quickly in CO_2 by bacterial remineralization (Oakes and Eyre, 2014). Indeed, DOC can also come from heterotrophic degradation of organic matter in the sediments (positive correlation between NH_4^+ and DOC) and be transferred to channel waters by tidal pumping during ebbing tide (Fig. 8).

A. Low/ebbing tide

Upstream salt ponds with macroalgae (Mayen et al., 2023)

Downstream coastal ocean with terrestrial inputs (Mayen et al., 2023)

NEE (autotrophy and CO_2 sink)

$GPP_{marsh} >>> R_{marsh}$

$GPP_{marsh} >>> R_{marsh}$

CO_2 sink

CO_2 sink

winter CO_2 emission
air pCO_2 < water pCO_2

spring/summer CO_2 sink
air pCO_2 > water pCO_2

Dyke

335 ± 214 ppmv
(6 - 721)

POC + DOC

O_2

NO_3^-

CO_2^{xx} 337 $\pm$ 330 ppmv
(89 - 1461)

CO_2

476 $\pm$ 168 ppmv
(270 - 1040)

DOC + POC
(max: spring/summer)

DIC + TA^x
(max: winter)

Heterotrophic processes

NH_4^+ + DIP
(max: winter)

Tidal pumping-driven porewater carbon fluxes ?

SO_4^{3-}

CO_2-undersaturated salt pond waters exported to the channel at low and ebbing tides

^{x} *Both aerobic and anaerobic respirations produce DIC; only anaerobic respiration produces TA (Krumins et al., 2013)*

^{xx} *Only aerobic respiration increases water pCO_2*

B. High/flooding tide

Upstream salt ponds with macroalgae (Mayen et al., 2023)

Downstream coastal ocean with terrestrial inputs (Mayen et al., 2023)

NEE (autotrophy and CO_2 sink)

$GPP_{marsh} >>> R_{marsh}$

$GPP_{marsh} > R_{marsh}$

CO_2 sink

spring CO_2 sink

winter, summer, fall CO_2 emission

CO_2 emission

Dyke

335 ± 214 ppmv
(6 - 721)

NO_3^-

CO_2^{xx} 455 $\pm$ 90 ppmv
(258 - 776)

CO_2

DIC

$NEP_{tot} < 0$

POC + DOC

O_2

NO_3^-

DOC + POC
(max: spring/summer)

DIC + TA^x
(max: winter)

Heterotrophic processes

Benthic DIC effluxes ?

NH_4^+ + DIP
(max: winter)

476 $\pm$ 168 ppmv
(270 - 1040)

SO_4^{3-}

CO_2-oversaturated coastal waters imported to the salt marsh at high and flooding tides

615

25

Fig. 8. Water inorganic carbon dynamics and atmospheric CO_2 fluxes at the studied salt marsh at two contrasted tidal periods: (A) low and ebbing tides (marsh emersion and channel waters coming from autochthonous porewater-drainage processes by tidal pumping and allochthonous waterflow from upstream salt ponds) and (B) high and flooding tides (marsh immersion by downstream coastal waters). Green arrows indicate autotrophic processes while brown arrows indicate heterotrophic processes. Dotted lines correspond to vertical carbon fluxes at the sediment-water and water-air interfaces by diffusion. Large half-circle arrows represent GPP_{marsh} and R_{marsh} balance measured by atmospheric Eddy Covariance inside the footprint while large vertical arrows represent net ecosystem CO_2 exchanges (NEE). During low and ebbing tides (A), the intense autotrophy of emerged plants and benthic microalgae induces the largest marsh CO_2 sink at the ecosystem scale with weak influence of channel water CO_2 fluxes. During high and flooding tides (B), GPP of emerged plants located on the highest marsh areas maintain a net marsh CO_2 sink at the ecosystem scale despite large R_{eco} fluxes from coastal waters (water-air CO_2 source). At high tide, negative NEP_{tot} rates in the water column correspond to aquatic heterotrophy (net DIC increases). Question marks correspond to uncertainties with regards to the contribution of (A) porewater advection to the channel by tidal pumping during low and ebbing tides (porewaters enriched in DIC, TA and nutrients in winter and porewaters enriched in DOC and depleted in CO_2 in spring) and (B) benthic DIC effluxes from sediments to water column by diffusion during high and flooding tides. The black frame at each situation (A, B) delimits the studied salt marsh through the one-point sampling location in relationships with upstream and downstream end-members previously studied (Mayen et al., 2023, 2024).

In spring and summer at low tide, the strong daytime increases (up to 190%) and night-time decreases (down to 10%) of DO in channel waters (Fig. 2) could indicate an intense biological activity of allochthonous aquatic macroalgae and/or autochthonous benthic microalgae which have higher rates of production and respiration than phytoplankton per unit area (Borum and Sand-Jensen, 1996; Hill et al., 2015). The fast-growing macroalgae recorded in the upstream salt ponds induced and maintained large water CO_2 undersaturation at both day and night, especially during warm and bright periods, inducing low diurnal variations of water pCO_2 (Mayen et al., 2023). Thus, these allochthonous macroalgae could also largely contributed to the large CO_2 uptake and DOC production recorded in the sampling channel that receives all upstream salt pond waters at low and ebb tides (Fig. 8). Previous studies have reported that macroalgae primary production favours tidal DOC exportations, a part of which can be sequestered in marine sediments (Hill et al., 2015; Krause-Jensen and Duarte, 2016; Raven, 2018).

Finally, the strong primary production of emerged plants, especially in spring and summer (high daytime GPP_{marsh} rates; Fig. 2) and confirmed by Mayen et al. (2024), could also induce DOC production through above-ground and belowground litter loss and root exudations (Kristensen and Alongi, 2006; Schiebel et al., 2018), then exported to surface waters by tidal pumping (Santos et al., 2019) inducing the highest DOC concentrations at low tide (Fig. 7). Most of the DOC leached from marsh plants, like *S. maritima*, is labile and biodegradable through bacterial activity, especially polysaccharides. However, because of its long residence time, lignin-derived DOC is a potentially important source of recalcitrant humic substances in marsh-influenced waters (Arnaud et al., 2024; Moran and Hodson, 1990; Wang et al., 2014). Thus, over our spring and summer 24-h cycles, the CO_2-depleted and DOC-concentrated water exportations from high to low tide could highlight the major role of autochthonous and allochthonous marsh primary production within all compartments (terrestrial and aquatic) in the coastal carbon cycle. However, in some cases, it is difficult to distinguish the relative contribution of allochthonous and autochthonous metabolic processes to water carbon dynamics recorded in the channel as both process origins are involved (Fig. 8). Contrary to our study, Santos at al. (2021) indicated large DIC and DOC outwelling from salt marshes over all seasons; it could indicate lower aquatic heterotrophy and higher aquatic autotrophy at our studied marsh, especially in spring and summer, allowing simultaneously large CO_2 uptake and DOC production.

4.3. Marsh aquatic respiration as DIC source

Large tidal variations of DIC and TA were recorded along the salinity gradient (Fig. 6-A) confirming a strong control of water mixing processes occurring in the channel on the carbonate chemistry (Reithmaier et al., 2023). However, the slope of this relationship was negative in C1-winter/C4-fall and positive in C2-spring/C3-summer due to a seasonal shift in channel salinity. More precisely, in the upstream salt ponds supplying the studied marsh channel during low tide, large seasonal variations of salinity exist due to different meteorological conditions and water managements inducing low salinity in winter/fall due to salt water dilution by the rain and high salinity in spring/summer due to salt water evaporation by the heat (Mayen et al., 2023). Due to this complexity, salinity could be a less straightforward tracer of water mixing processes in such salt marsh systems. During high tide (marsh immersion), total aquatic metabolism was heterotroph ($NEP_{tot} < 0$) both during day and night (except in spring at day) inducing net DIC and pCO_2 increases in water (Table 2 and Fig. 8-B). At the same time, the low contribution of planktonic aquatic metabolism (NEP_{pk}) to total aquatic metabolism (NEP_{tot}) suggested a major influence of benthic respiration processes on the water inorganic carbon pool. Previous studies in intertidal wetlands showed that benthic respiration produces strong sediment-to-water DIC fluxes through diffusion during immersion inducing water CO_2 oversaturation (Table 5) (Gong et al., 2023; Song et al., 2023).

During low tide (marsh emersion), the largest DIC and TA increases were measured in channel waters, especially in winter, highlighting a strong control of tidal forcing on water carbonate chemistry (Fig. 8-A). In similar salt marsh systems, the same tidal DIC pattern was recorded over all seasons with highest concentrations at low tide and lowest ones at high tide (Table 5). In most intertidal systems, such as salt marshes and mangroves, intense respiration processes occur in water-saturated muddy sediments inducing high DIC and TA concentrations in surface waters, especially at low tide through porewater exports driven by the tide (Nakamura et al., 2024; Reithmaier et al., 2023). In winter, during low autotrophic activity of *S. maritima* (Mayen et al., 2024), the highest POC:PON and POC:Chl*a* ratios measured at low tide (Fig. 7) suggested predominant detrital organic matter from decaying vegetation (Savoye et al., 2003). The less-depleted POC-δ^{13}C measured in winter at low tide (-14.6 ± 0.9‰; unpublished data) confirm the presence of terrestrial C4 plants in channel waters, like *S. maritima* (Amann et al., 2024). The impermeable muddy sediment section at the benthic interface, saturated in porewaters and enriched in plant-derived organic matter, constitute an energy source for heterotrophic microbial activity inducing, in turn, the largest increase of DIC and pCO_2 measured at low tide night (up to 3963 µmol kg^{-1} and 1461 ppmv, respectively; Fig. 6-B). During this period, DIC increased faster than TA until reaching very close concentrations (Table 1). This could indicate that most of carbonate ions (CO_3^{2-}) in channel waters were converted into bicarbonate ions (HCO_3^-) by the large addition of CO_2 and H^+ from marsh respiration processes, such that carbonate species in the exported channel waters mostly consisted of HCO_3^- and dissolved CO_2. In mangroves, Cabral et al. (2024) also confirmed a strong control of tidal forcing in water pCO_2 dynamics with highest values recorded a low tide during the highest tidal amplitudes. In addition, in our case, the strong DIP and NH_4^+ increases from high to low tide could confirm microbial respiration of organic matter in marsh sediments and, in turn, lateral export of DIC from porewaters to channel waters by tidal pumping (Fig. 8-A) as observed in other tidal systems (Cabral et al., 2024; Deborde et al., 2008; Santos et al., 2019). As coastal sediments are

anoxic from first millimetres (Wiebe et al., 1981), anaerobic respirations can be the dominant metabolic processes in salt marshes allowing DIC and TA outwelling (Reithmaier et al., 2023; Wang et al., 2016). In winter and fall, the nTA:nDIC regression slope (Fig. 6-B) suggests a major contribution of sulphate reduction to DIC and TA additions according to theorical stoichiometric ratios (Krumins et al., 2013). As sulphates are abundant in coastal waters, sulphate reduction is considered as among the most important organic carbon mineralisation pathways in salt marshes (Santos et al., 2021; Reithmaier et al., 2023; Wang et al., 2018). However, nutrient variations over our 24-h cycles could highlight other anaerobic processes, particularly at benthic interface, involving DIC and TA production in channel waters. In winter at high tide, we recorded the highest concentrations of $NO_3^-\_NO_2^-$ in coastal waters derived from riverine inputs (Belin et al., 2021). Over this 24-h cycle, the large $NO_3^-\_NO_2^-$ decrease (sink) from high to low tide was significantly related to the large NH_4^+ increase (source) ($R^2 = 0.90$, $p < 0.001$). This strong relationship could highlight a dissimilatory nitrate reduction to ammonium (DNRA) in sediments which is known to be an important metabolic process in salt marshes producing DIC and TA (Giblin et al., 2013; Hopkinson and Giblin, 2008). In low winter autotrophy conditions, $NO_3^-\_NO_2^-$ was not consumed by primary producers and could diffuse through sediments during immersion (Boynton et al., 2018) where it could be reduced in NH_4^+ by DNRA (Koop-Jakobsen and Giblin, 2010) before diffusing to channel waters through tidal pumping (Zheng et al., 2016). Direct measurements of anaerobic processes at the benthic interface, such as sulfate reduction and DNRA, should be assessed to confirm the significance of these metabolic processes in the winter DIC production at the studied site.

In spring and summer, lower tidal variations of DIC and TA were measured (Fig. 6-A). Contrary to winter and fall, the lowest nDIC and nTA in spring and summer were recorded at low tide associated with the lowest water pCO_2 (Fig. 6-B) indicating high primary production and low anaerobic respiration in the marsh channel. The regression lines between nTA and nDIC were significant but the slopes were lower than the theorical stoichiometric ratios of denitrification and sulfate reduction (Krumins et al., 2013). It could confirm that aerobic respiration and photosynthesis took place during these productive seasons and contributed mainly to DIC variations. However, in summer at low tide, the highest planktonic respiration (R_{pk}) associated with high POC:Chl$a$ ratios (> 300 mg mg^{-1}) and POC:PON ratios close to the Redfield value could suggest a large contribution of detrital phytoplanktonic biomass to DIC, DIP and DSi increases at the benthic interface, especially at night (Borawska et al., 2022; Boynton et al., 2018). However, this summer aquatic/benthic respiration in the channel was probably counterbalanced by the more intense autochthonous/allochthonous primary production (benthic microalgae and macroalgae) allowing to maintain large water CO_2 undersaturation at low tide (see section 4.2). In this salt marsh, a shift from plant decomposed organic matter in winter to labile fresh phytoplankton in spring/summer occurred.

4.4. Influence of aquatic and benthic metabolisms on NEE

For an integrative study of the planktonic community contribution to marsh CO_2 uptake including both high and low tide periods, daily C balances were computed from planktonic aquatic metabolism (NEP_{pk}) and net ecosystem CO_2 exchanges (NEE) within the EC footprint (Table 4). Over our 24-h cycles, planktonic metabolism was net autotrophic in winter and spring due to higher daytime CO_2 uptake than night-time CO_2 source in waters, whereas it was net heterotrophic in summer

and fall due to lower daytime CO_2 uptake than night-time CO_2 source. Simultaneously, at each season, NEE measurements indicated an intense autotrophy of the whole salt marsh at the ecosystem scale (Mayen et al., 2024) allowing a large atmospheric C uptake with a major contribution from emerged marsh plants (NEE_{marsh}) and a minor one from planktonic communities (NEP_{pk}) (Table 4). In spring, immersion reduced marsh C uptake (NEE_{marsh} - NEE = -0.76 g C m^{-2} d^{-1}) despite planktonic autotrophy whereas in summer, immersion slightly increased marsh C uptake (NEE_{marsh} - NEE = 0.20 g C m^{-2} d^{-1}) despite planktonic heterotrophy. Therefore, during our 24-h cycles, the study could indicate overall a low contribution of planktonic communities to marsh atmospheric C balances at the ecosystem scale accounting for up to 10% in spring. Moreover, NEE partitioning allowed to study the influence of benthic metabolism on marsh uptake/emission fluxes. Within our footprint, the low R_{marsh}:GPP_{marsh} ratio in winter (i.e. 0.26) suggested a weak influence of emerged sediment respiration on net marsh C uptake at the ecosystem scale; on the contrary, the higher R_{marsh}:GPP_{marsh} ratio in summer (i.e. 0.42) could indicate a significant influence of sediment respiration on marsh C uptake (Table 4). In an intertidal wetland (China), Gong et al. (2023) showed that microbial respiration increased DIC in sediments at low tide and induced large atmospheric CO_2 emissions from emerged sediments (0.95 ± 0.24 g C m^{-2} d^{-1}).

During high tide, downstream coastal waters immersed the salt marsh (mudflats and plants) and quickly disrupted NEE since water created a physical barrier between the soil and the atmosphere limiting CO_2 diffusion (Mayen et al., 2024; Polsenaere et al., 2012). In our study, water-air CO_2 fluxes estimated from water pCO_2 could be compared with NEE measured simultaneously by EC to go further into the contribution of aquatic metabolism on uptake/emission fluxes at the ecosystem scale (Table 2 and Fig. 8). During the highest immersion levels of plants (winter and spring), total aquatic metabolism and associated water-air CO_2 fluxes significantly influenced the overall marsh CO_2 exchanges within the footprint. Indeed, during daytime immersion in winter, aquatic heterotrophy (NEP_{tot} < 0) and associated water CO_2 oversaturation (atmospheric source) strongly reduced marsh CO_2 uptake measured by EC (NEE ≠ NEE_{marsh}; Fig. 2) whereas in spring, aquatic autotrophy (NEP_{tot} > 0) and associated water CO_2 undersaturation (atmospheric sink) allowed to maintain a weak marsh CO_2 uptake associated with a low GPP_{marsh} from *S. vera* on the highest marsh levels (Fig. 2). On the contrary, during the lowest immersion levels of plants (summer), aquatic heterotrophy (NEP_{tot} < 0) and associated water CO_2 oversaturation (atmospheric source) did not significantly influence marsh CO_2 uptake (NEE = NEE_{marsh}; Fig. 2) which was mainly controlled by emerged plants (*S. vera*) more represented during this marsh situation. During night-time, tidal immersion completely suppressed marsh CO_2 emissions from ecosystem respiration (plants and sediments) even causing a change in atmospheric CO_2 flux direction from source to sink in winter despite aquatic heterotrophy and water CO_2 oversaturation (Table 2). This weak night-time CO_2 uptake measured by EC during marsh immersion, as described in Mayen et al. (2024), could suggest important spatial water mass variations. Indeed, CO_2 undersaturated waters not measured at our single CO_2 sensor location but coming with the flood tide in the footprint could be related to coastal phytoplankton bloom development downstream the marsh and influence NEE as observed over a tidal bay nearby (Polsenaere et al., 2012). At our marsh, in spring 2022, an atmospheric CO_2 sink was recorded during night-time immersion and could be related to a centric diatom bloom (≈ 1.10^6 cell L^{-1}) seen few days earlier in the downstream shelf waters (Belin et al., 2021). In general, besides

these specific events, NEE at high tide remained strongly controlled by marsh vegetation, since emerged plants located on the highest levels can maintain daytime and night-time atmospheric CO_2 uptake or emission, respectively, even in the presence of coastal water oversaturated or undersaturated in CO_2.

5. Conclusions and limitations

Over the seasonal 24-h cycles, water pCO_2 dynamics was partly controlled by tidal forcing inducing intense variations in channel waters during transient tidal phases due to contrasted end-members (coastal water CO_2 oversaturation *versus* marsh water CO_2 undersaturation). In general, at high tide, water column CO_2 oversaturation, due to CO_2-concentrated coastal water input and marsh aquatic heterotrophy, was able to significantly reduce atmospheric CO_2 uptake measured by Eddy Covariance at the ecosystem scale (NEE) during the highest immersion levels only. Moreover, the water physical barrier between the marsh and the atmosphere can limit plant CO_2 uptake. From high to low tide, the salt marsh acted as a source of DIC, TA and NH_4^+, especially in winter, related to intense anaerobic respiration processes in waters and sediments inducing a significant increase in water pCO_2. On the contrary, in spring and summer, intense autochthonous and allochthonous primary production, including phytoplankton, benthic microalgae and macroalgae, induced the lowest water pCO_2 in the channel both at day and night, coupled with high DOC production. The spring/summer phytoplanktonic bloom measured in channel waters and the associated aquatic autotrophy led to CO_2-depleted water exportations downstream. However, at the daily scale, planktonic metabolism did not play a significant role in marsh atmospheric carbon balance measured by Eddy Covariance at the ecosystem scale (within the footprint). These results highlight that horizontal exchanges of coastal waters occurring at small timescales (diurnal and tidal) within salt marshes can significantly influence water carbon dynamics and associated atmospheric CO_2 fluxes over these dynamics blue carbon ecosystems and need to be specifically addressed and taken into account in regional and global coastal carbon study and balance.

In this study, the same diurnal/tidal synchronism (low and high tides at the same period of the day) was adopted during each 24-h cycle. However, due to the strong intraseasonal variability of meteorological (temperature, light, humidity, wind) and tidal (water level and immersion time) parameters, production and respiration rates in the marsh could strongly change from day to day and influenced the marsh carbon cycle differently. Thus, several 24-hour cycles per season with different meteorological and tidal conditions would allow to better take into account all temporal variabilities and to truly extrapolate at the seasonal scale our results on carbon dynamics in salt marshes. Direct measurements of benthic processes and fluxes, such as heterotrophic respiration in marsh sediments along with simultaneously sampling stations at different locations along the upstream ponds – salt marsh – downstream shelf, could better constrain the contribution of autochthonous metabolic processes at the benthic interface in the channel DIC production in comparison with allochthonous processes/inputs. Finally, lateral carbon exchanges and fluxes between marsh and end-member waters along with carbon sequestration rates should be put together with other measured fluxes at exchange interfaces and compartments to propose a first regional carbon budget of the studied tidal marsh and discussed among other regional and global carbon cycles.

Data availability

All raw data can be provided by the corresponding authors upon request.

795

Author Contribution Statements

PP, ARG, PS and JM designed the study. PP, ARG and PS obtained the funding acquisition. JM, PP and JD performed water samplings and measurements over all 24-hour cycles and ARG, MA and PK occasionally participated in fieldwork. JM, KC, YLM and EF performed labwork. JM investigated and processed the data. PP, PS, ARG, LA, VO and EL provide resources

800 in data analysis. JM, PP, ARG, PS and GA validated the data. JM made the graphics, wrote the draft and reviewed the manuscript. JM, PP, ARG, PS and GA led the review process assisted by MA, VO and JD.

Competing interests

The authors declare that they have no conflict of interest.

805

References

820 Adame, M. F., Cormier, N., Taillardat, P., Iram, N., Rovai, A., Sloey, T. M., Yando, E. S., Blanco-Libreros, J. F., Arnaud, M., Jennerjahn, T., Lovelock, C. E., Friess, D., Reithmaier, G. M. S., Buelow, C. A., Muhammad-Nor, S. M., Twilley, R. R., and Ribeiro, R. A.: Deconstructing the mangrove carbon cycle: Gains, transformation, and losses, Ecosphere, 15, e4806, https://doi.org/10.1002/ecs2.4806, 2024.

Alongi, D. M.: Carbon Balance in Salt Marsh and Mangrove Ecosystems: A Global Synthesis, JMSE, 8, 767,
825 https://doi.org/10.3390/jmse8100767, 2020.

Amann, B., Chaumillon, E., Bertin, X., Pignon-Mussaud, C., Marie-Claire, M.-C., Dupuy, C., Nathalie, L., and Sabine, S.: Understanding sediment and carbon accumulation in macrotidal minerogenic saltmarshes for climate resilience, Geomorphology, 467, 109465, https://doi.org/10.1016/j.geomorph.2024.109465, 2024.

Aminot, A. and Kérouel, R.: Hydrologie des écosystèmes marins: paramètres et analyses, Editions Quae, Versailles, France, 2004.

Aminot, A. and Kérouel, R.: Dosage automatique des nutriments dans les eaux marines : méthodes en flux continu, Editions Ifremer, méthodes d'analyse en milieu marin, 188 pp., 2007.

Arnaud, M., Bakhos, M., Rumpel, C., Dignac, M.-F., Bottinelli, N., Norby, R. J., Geairon, P., Deborde, J., Kostyrka, P., Gernigon, J., Lemesle, J.-C., and Polsenaere, P.: Salt marsh litter decomposition varies more by litter type than by extent of sea-level inundation, Commun Earth Environ, 5, 686, https://doi.org/10.1038/s43247-024-01855-0, 2024.

Bauer, J. E., Cai, W.-J., Raymond, P. A., Bianchi, T. S., Hopkinson, C. S., and Regnier, P. A. G.: The changing carbon cycle of the coastal ocean, Nature, 504, 61–70, https://doi.org/10.1038/nature12857, 2013.

Belin, C., Soudant, D., and Amzil, Z.: Three decades of data on phytoplankton and phycotoxins on the French coast: Lessons from REPHY and REPHYTOX. Harmful Algae 102, 101733. https://doi.org/10.1016/j.hal.2019.101733; 2021.

Borawska, Z., Szymczycha, B., Silberberger, M. J., Koziorowska-Makuch, K., Szczepanek, M., and Kędra, M.: Benthic fluxes of dissolved silica are an important component of the marine Si cycle in the coastal zone, Estuarine, Coastal and Shelf Science, 273, 107880, https://doi.org/10.1016/j.ecss.2022.107880, 2022.

Borges, A. V., Djenidi, S., Lacroix, G., Théate, J., Delille, B., and Frankignoulle, M.: Atmospheric CO_2 flux from mangrove surrounding waters, Geophysical Research Letters, 30, 2003GL017143, https://doi.org/10.1029/2003GL017143, 2003.

Borum, J. and Sand-Jensen, K.: Is Total Primary Production in Shallow Coastal Marine Waters Stimulated by Nitrogen Loading?, Oikos, 76, 406, https://doi.org/10.2307/3546213, 1996.

Boynton, W. R., Ceballos, M. A. C., Bailey, E. M., Hodgkins, C. L. S., Humphrey, J. L., and Testa, J. M.: Oxygen and Nutrient Exchanges at the Sediment-Water Interface: a Global Synthesis and Critique of Estuarine and Coastal Data, Estuaries and Coasts, 41, 301–333, https://doi.org/10.1007/s12237-017-0275-5, 2018.

Burgos, M., Ortega, T., and Forja, J.: Carbon Dioxide and Methane Dynamics in Three Coastal Systems of Cadiz Bay (SW Spain), Estuaries and Coasts, 41, 1069–1088, https://doi.org/10.1007/s12237-017-0330-2, 2018.

Cabral, A., Yau, Y. Y. Y., Reithmaier, G. M. S., Cotovicz, L. C., Barreira, J., Broström, G., Viana, B., Fonseca, A. L., and Santos, I. R.: Tidally driven porewater exchange and diel cycles control CO_2 fluxes in mangroves on local and global scales, Geochimica et Cosmochimica Acta, 374, 121–135, https://doi.org/10.1016/j.gca.2024.04.020, 2024.

Caffrey, J. M.: Factors controlling net ecosystem metabolism in U.S. estuaries, Estuaries, 27, 90–101, https://doi.org/10.1007/BF02803563, 2004.

Cai, W.-J.: Estuarine and Coastal Ocean Carbon Paradox: CO_2 Sinks or Sites of Terrestrial Carbon Incineration?, Annu. Rev. Mar. Sci., 3, 123–145, https://doi.org/10.1146/annurev-marine-120709-142723, 2011.

Carpenter, J. H.: The accuracy of the Winkler method for dissolved oxygen analysis, Limnol. Oceanogr., 10, 135–140, 1965.

Carrit, D. E. and Carpenter, J. H.: Comparison and evaluation of currently employed modifications of the Winkler method for determining dissolved oxygen in sea-water, J. Mar. Res., 24, 286–318, 1966.

Chapin, F. S., Woodwell, G. M., Randerson, J. T., Rastetter, E. B., Lovett, G. M., Baldocchi, D. D., Clark, D. A., Harmon, M. E., Schimel, D. S., Valentini, R., Wirth, C., Aber, J. D., Cole, J. J., Goulden, M. L., Harden, J. W., Heimann, M., Howarth, R. W., Matson, P. A., McGuire, A. D., Melillo, J. M., Mooney, H. A., Neff, J. C., Houghton, R. A., Pace, M. L., Ryan, M. G., Running, S. W., Sala, O. E., Schlesinger, W. H., and Schulze, E.-D.: Reconciling Carbon-cycle Concepts, Terminology, and Methods, Ecosystems, 9, 1041–1050, https://doi.org/10.1007/s10021-005-0105-7, 2006.

Chmura, G. L., Anisfeld, S. C., Cahoon, D. R., and Lynch, J. C.: Global carbon sequestration in tidal, saline wetland soils, Global Biogeochemical Cycles, 17, 2002GB001917, https://doi.org/10.1029/2002GB001917, 2003.

Cotovicz, L. C., Knoppers, B. A., Régis, C. R., Tremmel, D., Costa-Santos, S., and Abril, G.: Eutrophication overcoming carbonate precipitation in a tropical hypersaline coastal lagoon acting as a CO_2 sink (Araruama Lagoon, SE Brazil), Biogeochemistry, 156, 231–254, https://doi.org/10.1007/s10533-021-00842-3, 2021.

De Brouwer, J. and Stal, L.: Short-term dynamics in microphytobenthos distribution and associated extracellular carbohydrates in surface sediments of an intertidal mudflat, Mar. Ecol. Prog. Ser., 218, 33–44, https://doi.org/10.3354/meps218033, 2001.

Deborde, J., Anschutz, P., Auby, I., Glé, C., Commarieu, M.-V., Maurer, D., Lecroart, P., and Abril, G.: Role of tidal pumping on nutrient cycling in a temperate lagoon (Arcachon Bay, France), Marine Chemistry, 109, 98–114, https://doi.org/10.1016/j.marchem.2007.12.007, 2008.

Dickson, A. G.: Standard potential of the reaction: AgCl(s) + 1⁄2H_2(g) = Ag(s) + HCl$_{(aq)}$, and the standard acidity constant of the ion HSO_4 – in synthetic sea water from 273.15 to 318.15 K. Journal of Chemical Thermodynamics 22: 113–127, 1990.

Dickson, A. G., and Millero, F. J.: A comparison of the equilibrium constants for the dissociation of carbonic acid in seawater media. Deep-Sea Research 34: 1733–1743, 1987.

Dickson, A. G., Sabine, C. L., Christian, J. R., Bargeron, C. P., and North Pacific Marine Science Organization (Eds.): Guide to best practices for ocean CO_2 measurements, North Pacific Marine Science Organization, Sidney, BC, 1 pp., 2007.

Forbrich, I. and Giblin, A. E.: Marsh-atmosphere CO_2 exchange in a New England salt marsh, J. Geophys. Res. Biogeosci., 120, 1825–1838, https://doi.org/10.1002/2015JG003044, 2015.

Friedlingstein, P., O'Sullivan, M., Jones, M. W., Andrew, R. M., Bakker, D. C. E., Hauck, J., Landschützer, P., Le Quéré, C., Luijkx, I. T., Peters, G. P., Peters, W., Pongratz, J., Schwingshackl, C., Sitch, S., Canadell, J. G., Ciais, P., Jackson, R. B., Alin, S. R., Anthoni, P., Barbero, L., Bates, N. R., Becker, M., Bellouin, N., Decharme, B., Bopp, L., Brasika, I. B. M., Cadule, P., Chamberlain, M. A., Chandra, N., Chau, T.-T.-T., Chevallier, F., Chini, L. P., Cronin, M., Dou, X., Enyo, K., Evans, W., Falk, S., Feely, R. A., Feng, L., Ford, D. J., Gasser, T., Ghattas, J., Gkritzalis, T., Grassi, G., Gregor, L., Gruber, N., Gürses, Ö., Harris, I., Hefner, M., Heinke, J., Houghton, R. A., Hurtt, G. C., Iida, Y., Ilyina, T., Jacobson, A. R., Jain, A., Jarníková, T., Jersild, A., Jiang, F., Jin, Z., Joos, F., Kato, E., Keeling, R. F., Kennedy, D., Klein Goldewijk, K., Knauer, J., Korsbakken, J. I., Körtzinger, A., Lan, X., Lefèvre, N., Li, H., Liu, J., Liu, Z., Ma, L., Marland, G., Mayot, N., McGuire, P. C., McKinley, G. A., Meyer, G., Morgan, E. J., Munro, D. R., Nakaoka, S.-I., Niwa, Y., O'Brien, K. M., Olsen, A., Omar, A. M., Ono, T., Paulsen, M., Pierrot, D., Pocock, K., Poulter, B., Powis, C. M., Rehder, G., Resplandy, L., Robertson, E., Rödenbeck, C., Rosan, T. M., Schwinger, J., Séférian, R., et al.: Global Carbon Budget 2023, Earth Syst. Sci. Data, 15, 5301–5369, https://doi.org/10.5194/essd-15-5301-2023, 2023.

Friis, K., Körtzinger, A., and Wallace, D. W. R.: The salinity normalization of marine inorganic carbon chemistry data, Geophysical Research Letters, 30, 2002GL015898, https://doi.org/10.1029/2002GL015898, 2003.

Gazeau, F., Smith, S. V., Gentili, B., Frankignoulle, M., and Gattuso, J.-P.: The European coastal zone: characterization and first assessment of ecosystem metabolism, Estuarine, Coastal and Shelf Science, 60, 673–694, https://doi.org/10.1016/j.ecss.2004.03.007, 2004.

Giblin, A., Tobias, C., Song, B., Weston, N., Banta, G., and Rivera-Monroy, V.: The Importance of Dissimilatory Nitrate Reduction to Ammonium (DNRA) in the Nitrogen Cycle of Coastal Ecosystems, oceanog, 26, 124–131, https://doi.org/10.5670/oceanog.2013.54, 2013.

Gearing, J. N.: The use of stable isotope ratios of tracing the nearshore-offshore exchange of organic matter, in: Coastal-offshore ecosystem interactions, edited by: Jansson, B.-O., 69– 101, Springer-Verlag, Berlin, 1988.

Gran, G.: Determination of the equivalence point in potentiometric titrations Part II, The Analyst, 77, 661–671, https://doi.org/10.1039/AN9527700661, 1952.

Gong, J.-C., Li, B.-H., Hu, J.-W., Ding, X.-J., Liu, C.-Y., and Yang, G.-P.: Tidal effects on carbon dioxide emission dynamics in intertidal wetland sediments, Environmental Research, 238, 117110, https://doi.org/10.1016/j.envres.2023.117110, 2023.

Hill, R., Bellgrove, A., Macreadie, P. I., Petrou, K., Beardall, J., Steven, A., and Ralph, P. J.: Can macroalgae contribute to blue carbon? An Australian perspective: Can macroalgae contribute to blue carbon?, Limnol. Oceanogr., 60, 1689–1706, https://doi.org/10.1002/lno.10128, 2015.

Hopkinson, C. S. and Giblin, A. E.: Nitrogen Dynamics of Coastal Salt Marshes, in: Nitrogen in the Marine Environment, Elsevier, 991–1036, https://doi.org/10.1016/B978-0-12-372522-6.00022-0, 2008.

Jähne, B., Münnich, K. O., Bösinger, R., Dutzi, A., Huber, W., and Libner, P.: On the parameters influencing air-water gas exchange, J. Geophys. Res., 92, 1937–1949, https://doi.org/10.1029/JC092iC02p01937, 1987.

Jeong, H. J., Yoo, Y. D., Kim, J. S., Seong, K. A., Kang, N. S., and Kim, T. H.: Growth, feeding and ecological roles of the mixotrophic and heterotrophic dinoflagellates in marine planktonic food webs, Ocean Sci. J., 45, 65–91, https://doi.org/10.1007/s12601-010-0007-2, 2010.

Karl, D. M., Hebel, D. V., Björkman, K., and Letelier, R. M.: The role of dissolved organic matter release in the productivity of the oligotrophic North Pacific Ocean, Limnol. Oceanogr., 43, 1270–1286, https://doi.org/10.4319/lo.1998.43.6.1270, 1998.

Koné, Y. J.-M. and Borges, A. V.: Dissolved inorganic carbon dynamics in the waters surrounding forested mangroves of the Ca Mau Province (Vietnam), Estuarine, Coastal and Shelf Science, 77, 409–421, https://doi.org/10.1016/j.ecss.2007.10.001, 2008.

Koop-Jakobsen, K. and Giblin, A. E.: The effect of increased nitrate loading on nitrate reduction via denitrification and DNRA in salt marsh sediments, Limnol. Oceanogr., 55, 789–802, https://doi.org/10.4319/lo.2010.55.2.0789, 2010.

Kowalski, S., Sartore, M., Burlett, R., Berbigier, P., and Loustau, D.: The annual carbon budget of a French pine forest (*Pinus pinaster*) following harvest: ANNUAL CARBON BUDGET OF A PINE FOREST AFTER HARVEST, Global Change Biology, 9, 1051–1065, https://doi.org/10.1046/j.1365-2486.2003.00627.x, 2003.

Krause-Jensen, D. and Duarte, C. M.: Substantial role of macroalgae in marine carbon sequestration, Nature Geosci, 9, 737–742, https://doi.org/10.1038/ngeo2790, 2016.

Kristensen, E. and Alongi, D. M.: Control by fiddler crabs (Uca vocans) and plant roots (Avicennia marina) on carbon, iron, and sulfur biogeochemistry in mangrove sediment, Limnology & Oceanography, 51, 1557–1571, https://doi.org/10.4319/lo.2006.51.4.1557, 2006.

940 Krumins, V., Gehlen, M., Arndt, S., Van Cappellen, P., and Regnier, P.: Dissolved inorganic carbon and alkalinity fluxes from coastal marine sediments: model estimates for different shelf environments and sensitivity to global change, Biogeosciences, 10, 371–398, https://doi.org/10.5194/bg-10-371-2013, 2013.

Labasque, T., Chaumery, C., Aminot, A., and Kergoat, G.: Spectrophotometric Winkler determination of dissolved oxygen: re-examination of critical factors and reliability, Marine Chemistry, 88, 53–60, https://doi.org/10.1016/j.marchem.2004.03.004, 2004.

945 Laws, E. A.: Photosynthetic quotients, new production and net community production in the open ocean, Deep Sea Research Part A. Oceanographic Research Papers, 38, 143–167, https://doi.org/10.1016/0198-0149(91)90059-O, 1991.

Lee, K., Kim, T. W., Byrne, R. H., Millero, F. J., Feely, R. A., and Liu, Y. M.: The universal ratio of boron to chlorinity for the North Pacific and North Atlantic oceans. Geochimica et Cosmochimica Acta 74, 1801–1811. https://doi.org/10.1016/j.gca.2009.12.027, 2010.

950 Lewis, E. and Wallace, D.: Program developed for CO_2 system calculations. Carbon dioxide information analysis center. Oak Ridge National Laboratory, 1998.

Longhini, C. M., Souza, M. F. L., and Silva, A. M.: Net ecosystem production, calcification and CO_2 fluxes on a reef flat in Northeastern Brazil, Estuarine, Coastal and Shelf Science, 166, 13–23, https://doi.org/10.1016/j.ecss.2014.12.034, 2015.

Lorrain, A., Savoye, N., Chauvaud, L., Paulet, Y.-M., and Naulet, N.: Decarbonation and preservation method for the 955 analysis of organic C and N contents and stable isotope ratios of low-carbonated suspended particulate material, Analytica Chimica Acta, 491, 125–133, https://doi.org/10.1016/S0003-2670(03)00815-8, 2003.

Mayen, J., Polsenaere, P., Regaudie De Gioux, A., Dupuy, C., Vagner, M., Lemesle, J.-C., Poitevin, B., and Souchu, P.: Influence of typology and management practices on water pCO_2 and atmospheric CO_2 fluxes over two temperate shelf–estuary–marsh water continuums, Regional Studies in Marine Science, 67, 103209, 960 https://doi.org/10.1016/j.rsma.2023.103209, 2023.

Mayen, J., Polsenaere, P., Lamaud, É., Arnaud, M., Kostyrka, P., Bonnefond, J.-M., Geairon, P., Gernigon, J., Chassagne, R., Lacoue-Labarthe, T., Regaudie De Gioux, A., and Souchu, P.: Atmospheric CO_2 exchanges measured by eddy covariance over a temperate salt marsh and influence of environmental controlling factors, Biogeosciences, 21, 993–1016, https://doi.org/10.5194/bg-21-993-2024, 2024.

965 Mcleod, E., Chmura, G. L., Bouillon, S., Salm, R., Björk, M., Duarte, C. M., Lovelock, C. E., Schlesinger, W. H., and Silliman, B. R.: A blueprint for blue carbon: toward an improved understanding of the role of vegetated coastal habitats in sequestering CO_2, Frontiers in Ecol & Environ, 9, 552–560, https://doi.org/10.1890/110004, 2011.

Mehrbach, C., Culberson, C. H., Hawley, J. E., Pytkowicz, R. M.: Measurement of the Apparent Dissociation Constants of Carbonic Acid in Seawater at Atmospheric Pressure. Limnology and Oceanography 18, 897–907, 1973.

970 Migné, A., Gévaert, F., Créach, A., Spilmont, N., Chevalier, E., and Davoult, D.: Photosynthetic activity of intertidal microphytobenthic communities during emersion: in situ measurements of chlorophyll fluorescence (PAM) and CO_2 flux (IRGA) [1], Journal of Phycology, 43, 864–873, https://doi.org/10.1111/j.1529-8817.2007.00379.x, 2007.

Moran, M. and Hodson, R.: Contributions of degrading Spartina alterniflora lignocellulose to the dissolved organic carbon pool of a salt marsh, Mar. Ecol. Prog. Ser., 62, 161–168, https://doi.org/10.3354/meps062161, 1990.

975 Morelle, J., Roose-Amsaleg, C., and Laverman, A. M.: Microphytobenthos as a source of labile organic matter for denitrifying microbes, Estuarine, Coastal and Shelf Science, 275, 108006, https://doi.org/10.1016/j.ecss.2022.108006, 2022.

Nakamura, W., Phyo Thet Naing, Watanabe, K., Tokoro, T., Gempei, K., Endo, T., Kuwae, T., and Sasaki, J.: Changes in DIC/TA ratio by tidal asymmetry control pCO_2 over a spring-neap tidal cycle in a subtropical mangrove forest in Japan, Geochem. J., 58, 28–45, https://doi.org/10.2343/geochemj.gj24003, 2024.

980 Oakes, J. M. and Eyre, B. D.: Transformation and fate of microphytobenthos carbon in subtropical, intertidal sediments: potential for long-term carbon retention revealed by ^{13}C-labeling, Biogeosciences, 11, 1927–1940, https://doi.org/10.5194/bg-11-1927-2014, 2014.

Polsenaere, P., Lamaud, E., Lafon, V., Bonnefond, J.-M., Bretel, P., Delille, B., Deborde, J., Loustau, D., and Abril, G.: Spatial and temporal CO_2 exchanges measured by Eddy Covariance over a temperate intertidal flat and their relationships to 985 net ecosystem production, Biogeosciences, 9, 249–268, https://doi.org/10.5194/bg-9-249-2012, 2012.

Polsenaere, P., Delille, B., Poirier, D., Charbonnier, C., Deborde, J., Mouret, A., and Abril, G.: Seasonal, Diurnal, and Tidal Variations of Dissolved Inorganic Carbon and pCO2 in Surface Waters of a Temperate Coastal Lagoon (Arcachon, SW France), Estuaries and Coasts, https://doi.org/10.1007/s12237-022-01121-6, 2022.

Raven, J.: Blue carbon: past, present and future, with emphasis on macroalgae, Biol. Lett., 14, 20180336, 990 https://doi.org/10.1098/rsbl.2018.0336, 2018.

Razanamahandry, V. F., Borges, A. V., Brosens, L., Morana, C., Razafimbelo, T., Rafolisy, T., Govers, G., and Bouillon, S.: Biogeochemical functioning of Lake Alaotra (Madagascar): a reset of aquatic carbon sources along the land–ocean aquatic continuum, Biogeosciences, 22, 2403–2424, https://doi.org/10.5194/bg-22-2403-2025, 2025.

Reithmaier, G. M. S., Cabral, A., Akhand, A., Bogard, M. J., Borges, A. V., Bouillon, S., Burdige, D. J., Call, M., Chen, N., 995 Chen, X., Cotovicz, L. C., Eagle, M. J., Kristensen, E., Kroeger, K. D., Lu, Z., Maher, D. T., Pérez-Lloréns, J. L., Ray, R., Taillardat, P., Tamborski, J. J., Upstill-Goddard, R. C., Wang, F., Wang, Z. A., Xiao, K., Yau, Y. Y. Y., and Santos, I. R.: Carbonate chemistry and carbon sequestration driven by inorganic carbon outwelling from mangroves and saltmarshes, Nat Commun 14, 8196, https://doi.org/10.1038/s41467-023-44037-w, 2023.

Redfield, A. C.: The biological control of chemical factors in the environment, Am. Sci., 46, 205–221, 1958.

1000 Saderne, V., Baldry, K., Anton, A., Agustí, S., and Duarte, C. M.: Characterization of the CO_2 System in a Coral Reef, a Seagrass Meadow, and a Mangrove Forest in the Central Red Sea, JGR Oceans, 124, 7513–7528, https://doi.org/10.1029/2019JC015266, 2019.

Santos, I. R., Maher, D. T., Larkin, R., Webb, J. R., and Sanders, C. J.: Carbon outwelling and outgassing vs. burial in an estuarine tidal creek surrounded by mangrove and saltmarsh wetlands, Limnol. Oceanogr., 64, 996–1013, 1005 https://doi.org/10.1002/lno.11090, 2019.

Santos, I. R., Burdige, D. J., Jennerjahn, T. C., Bouillon, S., Cabral, A., Serrano, O., Wernberg, T., Filbee-Dexter, K., Guimond, J. A., and Tamborski, J. J.: The renaissance of Odum's outwelling hypothesis in "Blue Carbon" science, Estuarine, Coastal and Shelf Science, 255, 107361, https://doi.org/10.1016/j.ecss.2021.107361, 2021.

Savelli, R., Bertin, X., Orvain, F., Gernez, P., Dale, A., Coulombier, T., Pineau, P., Lachaussée, N., Polsenaere, P., Dupuy, C., and Le Fouest, V.: Impact of Chronic and Massive Resuspension Mechanisms on the Microphytobenthos Dynamics in a Temperate Intertidal Mudflat, J. Geophys. Res. Biogeosci., 124, 3752–3777, https://doi.org/10.1029/2019JG005369, 2019.

Savoye, N., Aminot, A., Tréguer, P., Fontugne, M., Naulet, N., and Kérouel, R.: Dynamics of particulate organic matter d[15]N and d[13]C during spring phytoplankton blooms in a macrotidal ecosystem (Bay of Seine, France). Mar. Ecol. Prog. Ser. 255: 27–41. doi:10.3354/meps255027, 2003.

Schäfer, K. V. R., Tripathee, R., Artigas, F., Morin, T. H., and Bohrer, G.: Carbon dioxide fluxes of an urban tidal marsh in the Hudson-Raritan estuary: Carbon dioxide fluxes of an wetland, J. Geophys. Res. Biogeosci., 119, 2065–2081, https://doi.org/10.1002/2014JG002703, 2014.

Schiebel, H. N., Gardner, G. B., Wang, X., Peri, F., and Chen, R. F.: Seasonal Export of Dissolved Organic Matter from a New England Salt Marsh, Journal of Coastal Research, 344, 939–954, https://doi.org/10.2112/JCOASTRES-D-16-00196.1, 2018.

Song, S., Wang, Z. A., Kroeger, K. D., Eagle, M., Chu, S. N., and Ge, J.: High-frequency variability of carbon dioxide fluxes in tidal water over a temperate salt marsh, Limnology & Oceanography, lno.12409, https://doi.org/10.1002/lno.12409, 2023.

Stoecker, D. K.: Mixotrophy among Dinoflagellates1, J Eukaryotic Microbiology, 46, 397–401, https://doi.org/10.1111/j.1550-7408.1999.tb04619.x, 1999.

Utermöhl, H.: Zur vervollkommnung der quantitativen phytoplankton methodik. Mitteilungen-Internationale Vereiningung fur Limnologie. 9, 1–38, 1958.

Van Boekel, W., Hansen, F., Riegman, R., and Bak, R.: Lysis-induced decline of a Phaeocystis spring bloom and coupling with the microbial foodweb, Mar. Ecol. Prog. Ser., 81, 269–276, https://doi.org/10.3354/meps081269, 1992.

Van Dam, B. R., Edson, J. B., and Tobias, C.: Parameterizing Air-Water Gas Exchange in the Shallow, Microtidal New River Estuary, JGR Biogeosciences, 124, 2351–2363, https://doi.org/10.1029/2018JG004908, 2019.

Wang, J., Yu, G., Han, L., Yao, Y., Sun, M., and Yan, Z.: Ecosystem carbon exchange across China's coastal wetlands: Spatial patterns, mechanisms, and magnitudes, Agricultural and Forest Meteorology, 345, 109859, https://doi.org/10.1016/j.agrformet.2023.109859, 2024.

Wang, S. R., Di Iorio, D., Cai, W., and Hopkinson, C. S.: Inorganic carbon and oxygen dynamics in a marsh-dominated estuary, Limnol. Oceanogr., 63, 47–71, https://doi.org/10.1002/lno.10614, 2018.

Wang, X., Chen, R. F., Cable, J. E., and Cherrier, J.: Leaching and microbial degradation of dissolved organic matter from salt marsh plants and seagrasses, Aquat Sci, 76, 595–609, https://doi.org/10.1007/s00027-014-0357-4, 2014.

Wang, Z. A. and Cai, W.-J.: Carbon dioxide degassing and inorganic carbon export from a marsh-dominated estuary (the Duplin River): A marsh CO_2 pump, Limnol. Oceanogr., 49, 341–354, https://doi.org/10.4319/lo.2004.49.2.0341, 2004.

Wang, Z. A., Kroeger, K. D., Ganju, N. K., Gonneea, M. E., and Chu, S. N.: Intertidal salt marshes as an important source of inorganic carbon to the coastal ocean, Limnol. Oceanogr., 61, 1916–1931, https://doi.org/10.1002/lno.10347, 2016.

Wei, S., Han, G., Jia, X., Song, W., Chu, X., He, W., Xia, J., and Wu, H.: Tidal effects on ecosystem CO_2 exchange at multiple timescales in a salt marsh in the Yellow River Delta, Estuarine, Coastal and Shelf Science, 238, 106727, https://doi.org/10.1016/j.ecss.2020.106727, 2020.

1045   Wiebe, W. J., Christian, R. R., Hansen, J. A., King, G., Sherr, B. and Skyring, G.: Anaerobic respiration and fermentation, p. 137–159. In L. R. Pomeroy, and R. G. Wiegert [eds.], The ecology of a salt marsh. Springer, 1981.

Wielgat-Rychert, M., Rychert, K., Witek, Z., and Zalewski, M.: CALCULATION OF THE PHOTOSYNTHETIC QUOTIENT (PQ) IN THE GULF OF GDAŃSK (SOUTHERN BALTIC), 2017.

Weiss, R.F.: Carbon dioxide in water and seawater: the solubility of a non-ideal gas. Marine Chemistry 2, 203–215.
1050   https://doi.org/10.1016/0304-4203(74)90015-2, 1974.

Xi, M., Zhang, X., Kong, F., Li, Y., Sui, X., and Wang, X.: CO_2 exchange under different vegetation covers in a coastal wetland of Jiaozhou Bay, China, Ecological Engineering, 137, 26–33, https://doi.org/10.1016/j.ecoleng.2018.12.025, 2019.

Zheng, Y., Hou, L., Liu, M., Liu, Z., Li, X., Lin, X., Yin, G., Gao, J., Yu, C., Wang, R., and Jiang, X.: Tidal pumping facilitates dissimilatory nitrate reduction in intertidal marshes, Sci Rep, 6, 21338, https://doi.org/10.1038/srep21338, 2016.

1055